KINEMATICS OF WATER PARTICLE MOTION WITHIN THE SURF ZONE

Rafael Steer

NAVAL POSTGRADUATE SCHOOL
Monterey, California

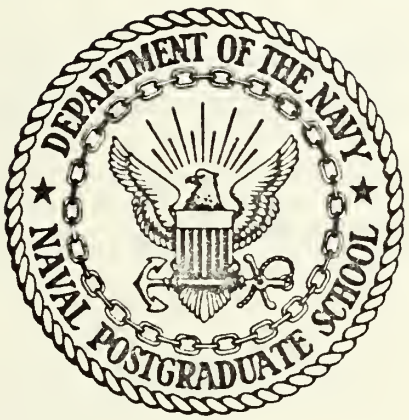

THESIS

Kinematics of Water Particle Motion
Within the Surf Zone

by

Rafael Steer

Advisor: E. B. Thornton

September 1972

Kinematics of Water Particle Motion

Within the Surf Zone

by

Rafael Steer
Lieutenant J.G., Colombian Navy

Submitted in partial fulfillment of the
requirements for the degree of

MASTER OF SCIENCE IN OCEANOGRAPHY

from the

NAVAL POSTGRADUATE SCHOOL
September 1972

ABSTRACT

Simultaneous measurements of sea surface elevation and horizontal and vertical particle velocities at 39 and 69 cm elevations in the column of water of 130 cm total depth were made inside the surf zone. Also, the offshore sea surface elevation at this location was measured for purposes of comparison. The velocities were measured using electromagnetic flow meters, and the sea surface elevation was measured using pressure wave gauges. Probability density functions, pdf, were determined for each record. The pdf's for the sea surface elevation and particle velocities inside the surf zone were highly skewed. Spectral computations show that the range of significant energy was between 0.05 and 0.6 hertz. The phase angle was compared to linear wave theory and shows a shifting of phase for the horizontal velocity with sea surface elevation from 0 degree at low frequency to 90 degrees at higher frequencies. The energy-density spectra show that the horizontal component is approximately 95% of the total kinetic energy of the surf zone. In the range of significant energy, a coherence of about 0.9 was found for the sea surface elevation and particle velocities which indicates that the particle motion inside the surf zone is for the most part wave-induced.

TABLE OF CONTENTS

LIST OF FIGURES

I. INTRODUCTION

A. REVIEW OF PREVIOUS WORKS

With reference to the surf zone only the more general features and characteristics of the motion of the fluid are at present understood. This is due to the lack of understanding of waves after the breaking point. Most of the knowledge at this time is based on approximations of wave theory or empirical relationships.

The difficulties are practical as well as theoretical. The surf zone is a very hostile environment to work in and a very difficult one to reproduce properly in the laboratory. Another major difficulty has been a lack of instrumentation to make velocity measurements for wave-induced motion and turbulence. Only a few experiments have been conducted to measure and study the kinematics of water particle motions due to waves in shallow and intermediate water, and almost none for the kinematics of water particle motion inside the surf zone itself.

Among the laboratory experiments the most notable is a study by Iversen (1953) in which photographic techniques were used to obtain a Lagrangian description of water particle motion. However, due to the slope of his model beach, spilling breakers were not considered.

Field measurements have been made by a number of authors using a variety of instruments. Inman (1956) measured the drag force to infer water particle motion. Walker (1969) used propeller type flow meters. Miller and Zeigler (1964) used meters based on acoustic principles;

they compared their measurements with higher order wave theory and found some qualitative agreement. Thornton (1969) used an electromagnetic flow meter and presented his results in the form of spectra. His results showed a gradual decay of energy across the surf zone and a shifting of energy to the higher frequency turbulent region of the spectrum.

Some attempts have been made to theoretically describe the kinematics of the surf zone. One of them by Collins (1970) describes the probability distribution functions of the wave characteristics of wave height and period for the region inside the surf utilizing the hydrodynamic relationships for shoaling and refraction.

B. OBJECTIVE

The objective of this research was to make preliminary studies on the kinematics of the water particle motion within the surf zone and within breaking waves. With this purpose in mind, simultaneous measurements were made of the instantaneous sea surface elevation and of horizontal and vertical particle velocities at different elevations in the same column of water in the surf zone, and of the offshore sea surface elevation. The probability density functions and spectra of the wave and particle velocity measurements were determined.

II. NATURE OF THE PROBLEM

A. CHARACTERISTICS OF THE SURF ZONE

Theories developed to describe characteristics of waves, such as wave height, period, and particle velocity, can be applied reasonably well to deep water waves, and with less accuracy to shoaling waves up to the point of near-breaking conditions. However, upon breaking the waves lose their ordered character and can no longer be described analytically. Each type of breaker, spilling, plunging, or surging, (depending upon the beach slope and deep water wave steepness) causes a different type of flow and consequently a different distribution of energy in the surf zone. Furthermore, moving boundaries at the bottom and surface of the sea together with the unsteady flow motion, make the surf zone a very difficult place for the application of a theoretical model.

However, results of experiments by Thornton (1969) suggest that the kinematics is not as disorganized as one might be led to believe. In order to develop a theoretical model it is necessary to have at least some *a priori* knowledge of the characteristics of the wave induced motion and the structure of the turbulence.

If it is desired to study the details of surf zone flow, it is necessary to have a very large model or to take measurements *in situ* with appropriate instruments for measuring instantaneous velocities. A limitation inherent in laboratory studies is space. The most commonly occurring breaking wave is of the spilling type which is observed on very flat beaches; this calls for very long wave tanks.

Direct field measurements can overcome these problems. A difficulty is that the large scale conditions peculiar only to the place where the data is taken may affect the mean flow in such a way that it is applicable only to a particular set of conditions. However, small scale features, such as turbulent motion in the breaking waves, are not affected directly by the large scale conditions and their study produces better results when done in the field. Furthermore, the process generally can be assumed to be stationary, that is, the mean and variance do not change with time. This is a good assumption for short measurements on the order of 20 minutes as done in this research.

In general, the surface waves and wave induced water particle motion have the characteristics of random phenomena, therefore it is necessary to utilize statistical procedures to describe them. The basic analyses and their application to the present problem are described in the following sections.

B. STATISTICAL ANALYSIS

1. Probability Density Function

The probability density function for random data describes the probability that a particular process will assume a value within some defined range at any instant of time. The probability that the sample time history record $x(t)$ assumes a value between x and $(x + \Delta x)$ will approach an exact probability description as the length of the sample record, T, approaches infinity, and as Δx approaches zero. In equation form:

$$p(x) = \lim_{\Delta x \to 0} \lim_{T \to \infty} \frac{1}{T} \left[\frac{T_i}{\Delta x} \right]$$

where T_i is the total amount of time that $x(t)$ falls inside the range $(x, x + \Delta x)$, and T is the total observation time. The probability density function is always a real, non-negative function.

2. Energy-Density Spectrum

The energy-density spectrum is computed from the Fourier transform of the auto-covariance function of the record time series. The auto-covariance function describes the general dependence of the values of the data at one time on the values at another time. It is expressed as a function of lag time τ as

$$\Phi_{11}(\tau) = \lim_{T \to \infty} \frac{1}{T} \int_{t}^{t+T} x_1(t)\, x_1(t+\tau)\, dt$$

The quantity $\Phi_{11}(\tau)$ is always a real-valued even-function, with a maximum at $\tau = 0$.

A Parzen lag window is applied to the covariance functions to account for the finite length of the record in computing the spectra. The Parzen lag window has the advantage of no negative side lobes and maintains the sample coherence between its theoretical values of 0 and 1. This eliminates any numerical instability problem that may arise in the analysis procedure, particularly when calculating cross-spectra. The Parzen lag window is given in Bendat and Piersol (1966) by the formula

$$P(\tau) = \begin{cases} 1 - 6\left(\frac{\tau}{T_m}\right)^2 + 6\left(\frac{\tau}{T_m}\right)^3 & \tau \leq \frac{T_m}{2} \\ 2\left[1 - \left(\frac{\tau}{T_m}\right)\right]^3 & \frac{T_m}{2} \leq \tau < T_m \\ 0 & \tau > T_m \end{cases}$$

where T_m is the total time lag.

The Fourier transform of the modified auto-covariance function is the energy-density spectrum, given by

$$\Phi_{11}(f) = \int_{-\infty}^{\infty} P(\tau)\,\Phi_{11}(\tau)\,e^{-i\,2\,\pi\,f\,\tau}\,d\tau$$

This spectrum describes the partitioning of energy-density by frequencies. The area under the wave height spectrum is proportional to the total potential energy-density of the sea surface elevation. The area under the curve of the velocity spectrum is proportional to the kinematic energy-density. In both cases the total area under the spectrum is equal to the mean square value of the random variable and therefore equal to the variance.

3. Cross-Spectral Density Function

The cross-spectral density is defined as the Fourier transform of the cross-covariance function. The cross-covariance function for two sets of random data describes the general dependence of the values of one set of data on the other. It is similar to the auto-covariance function except that two records are lagged against each other instead of a single record lagged against itself. The cross-covariance function

tends to the exact value as T approaches infinity. In equation form

$$\Phi_{12}(\tau) = \lim_{T \to \infty} \frac{1}{T} \int_{t}^{t+T} x_1(t)\, x_2(t+\tau)\, dt$$

The function $\Phi_{12}(\tau)$ is always a real-valued function, but does not necessarily have a maximum of $\tau = 0$, or is an even-function, as was the auto-covariance function.

The cross-spectral density function is expressed as

$$\Phi_{12}(f) = \int_{-\infty}^{\infty} P(\tau)\, \Phi_{12}(\tau)\, e^{-i 2 \pi f \tau}\, d\tau$$

where $P(\tau)$ is the Parzen function defined above.

Because the cross-correlation function is not an even-function, the cross-spectrum is generally complex and can be defined in terms of its real and imaginary parts

$$\Phi_{12}(f) = C_{12}(f) - jQ_{12}(f)$$

where the real part is called the co-spectrum

$$C_{12}(f) = 2 \int_{0}^{\infty} P(\tau)\, [\Phi_{12}(\tau) + \Phi_{12}(-\tau)] \cos(2 \pi f \tau)\, d\tau$$

and the imaginary part is called the quadrature-spectrum

$$Q_{12}(f) = 2 \int_{0}^{\infty} P(\tau)\, [\Phi_{12}(\tau) + \Phi_{12}(-\tau)] \sin(2 \pi f \tau)\, d\tau$$

4. Phase Angle

The cross-spectral density function can be expressed in complex polar notation as

$$\Phi_{12}(f) = \left|\Phi_{12}(f)\right| e^{-j \in_{12}(f)}$$

where the phase angle, $\in_{12}(f)$, is the average angular difference by which the cross-correlated components of $x_2(t)$ lead those of $x_1(t)$ in each spectral frequency band. The phase angle is calculated using the expression

$$\in_{12}(f) = \tan^{-1} \frac{Q_{12}(f)}{C_{12}(f)}$$

where $C_{12}(f)$ and $Q_{12}(f)$ are the cross-spectral components described above. The phase angle is bounded by the values $-\pi \leq \in_{12}(f) \leq \pi$

5. Coherence Function

The coherence function gives an expression for the correlation of two random variables as a function of frequency. It is defined by the equation

$$\gamma_{12}^2(f) = \frac{\left|\Phi_{12}(f)\right|^2}{\Phi_{11}(f)\,\Phi_{22}(f)}$$

and has a range of values

$$0 \leq \gamma_{12}^2(f) \leq 1$$

In the ideal case of two completely coherent records, $\gamma_{12}^2(f)$ has the maximum value of unity. As the correlation between the records decreases

the value of $\Upsilon^2_{12}(f)$ decreases, and reaches the minimum value of zero when the records are completely incoherent or statistically independent.

III. INSTRUMENTATION

A. FLOW METER

The water particle velocities were measured using two Engineering-Physics Company water current meters, type 6130, see Figure 1. The current meter operation is based on the electromagnetic induction principle. A symmetrical magnetic field is generated in the water by a driving coil imbedded in the probe. When water in the vicinity of the probe has a velocity relative to the magnetic field, an electric field is induced as expressed by the vector equation

$$\vec{E} = \vec{u} \times \vec{B}$$

where $\vec{E}$ is the induced electric potential, $\vec{B}$ is the magnetic field, and $\vec{u}$ is the water velocity.

The induced electric potential is sensed by two electrodes, in contact with the water, oriented in the same direction as the induced field. This produces a dc signal proportional to the magnitude of the velocity component perpendicular to the electrode's axis. Orthogonal components of the velocity are measured using two pairs of electrodes placed with axis perpendicular to each other.

The measureable range of velocities is from 0 to 1.5 m/sec with a maximum output error of one percent of full scale reading. The instrument has two electrical time constant settings, 0.3 or 1.0 seconds. The output rms noise level is a function of the electrical time constant and is given by the expression

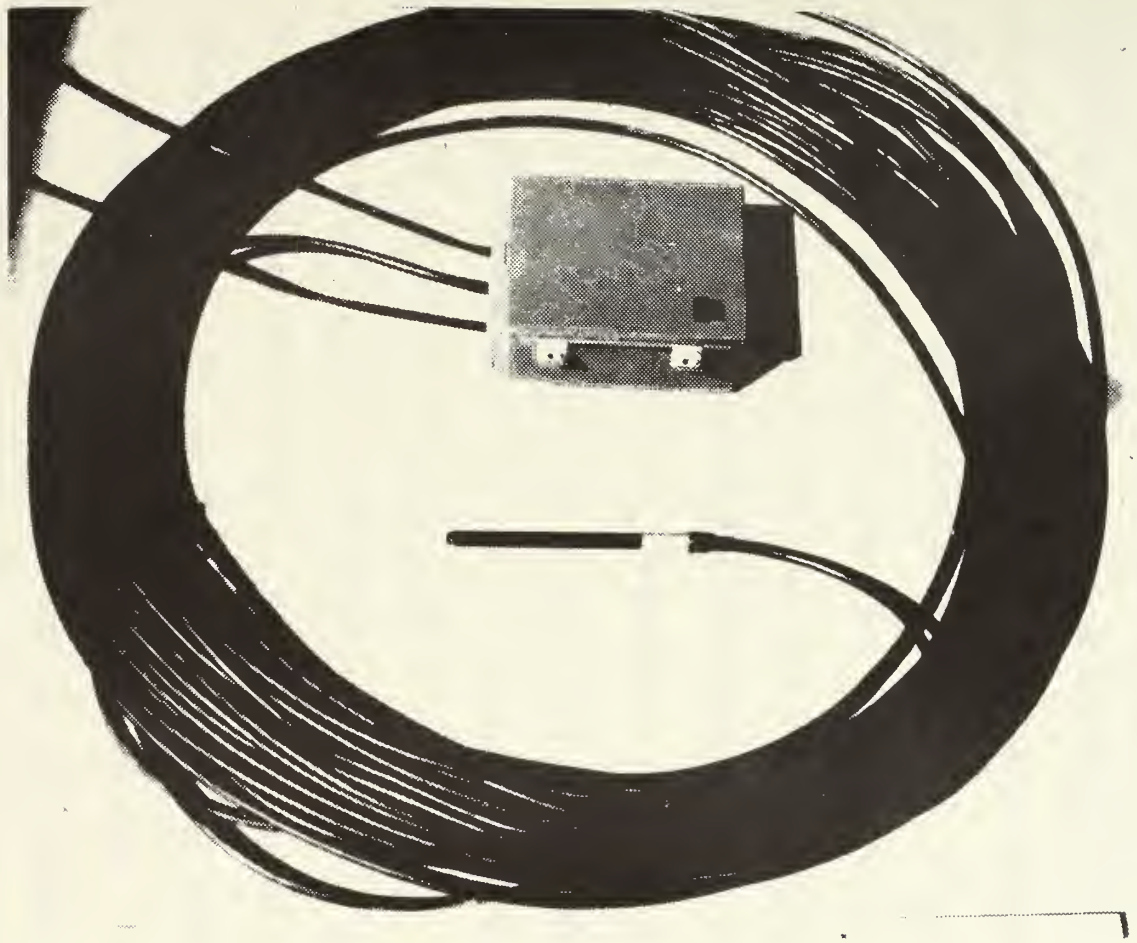

Electromagnetic Water Current Meter EPCO 6130.

Figure 1

$$\text{Random noise (rms)} = 0.015\ T_c^{-1/2} \quad \text{(feet/sec)}$$

where T_c is the electrical time constant. This relationship was validated during calibration.

The current meter is calibrated under steady flow conditions by the manufacturer but different characteristics are expected under unsteady flow conditions due to a change in the boundary layer on the face of the transducer. The probe was recalibrated by oscillating it in a water tank. The set-up is shown in Figure 2. The carriage on which the flow meter probe was mounted travels back and forth on rails. It is driven by an electric motor with a constant throw arm and variable rotation velocity. The peak carriage velocity was calculated from the tangential velocity of the motor arm. The ratio of carriage velocity, V_t, to the velocity measured by the instrument, V_m, was found for different angular velocities. This was done for each channel of the current meter by orienting each pair of electrodes perpendicular to the direction of flow respectively. The results are shown in Figures 3 and 4.

The ratio of V_m/V_t is also plotted as a function of the frequency of oscillation in Figures 5 and 6. The range of frequencies measured ranges from 0 to 0.5 Hz; the latter being the highest frequency which the carriage was capable of without becoming unstable. It is noticed that there is a decrease in the velocity ratio with increasing frequency. A measured response time, or time constant, can be calculated from the measurements. Using the usual definition, the response time

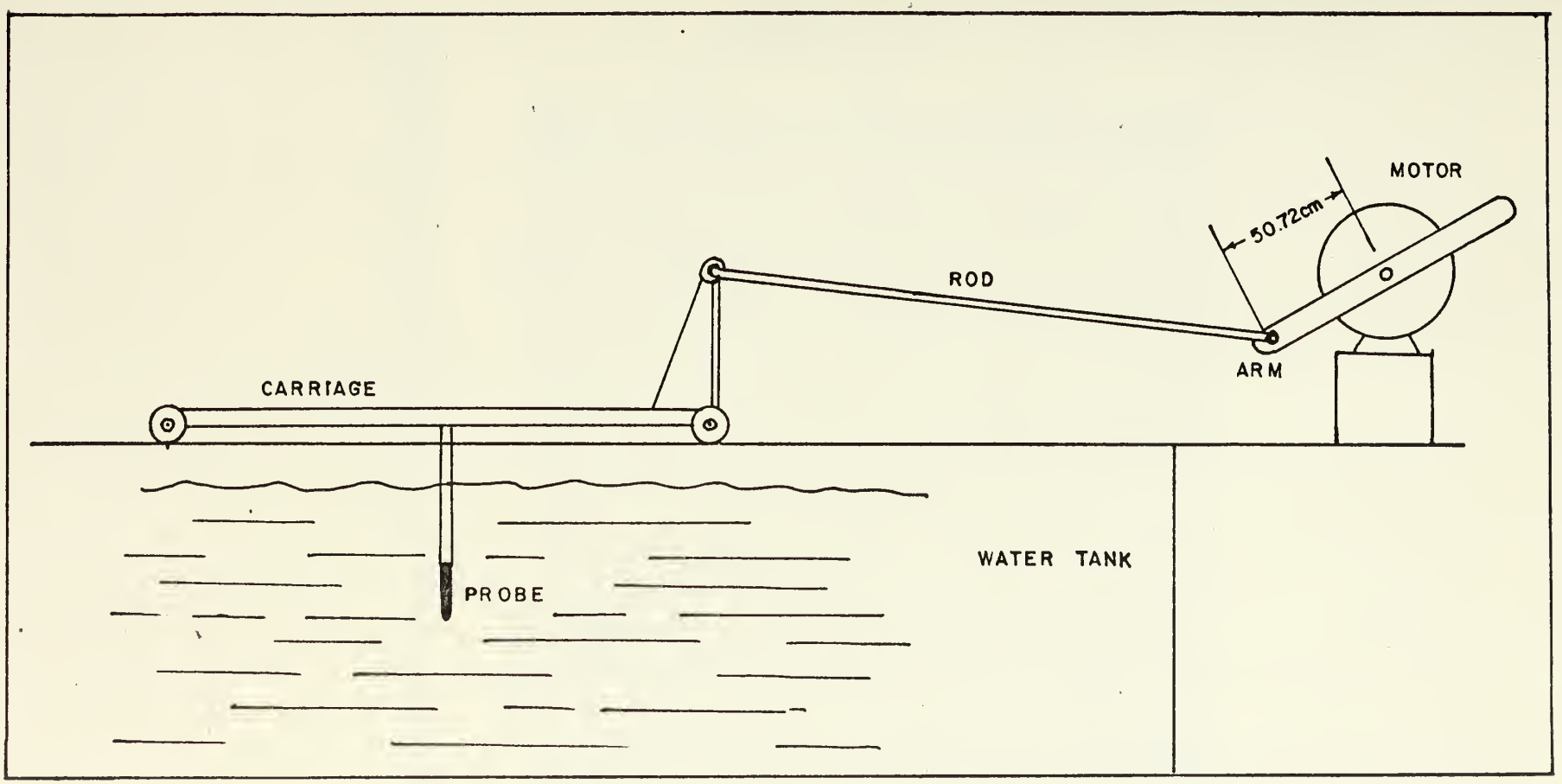

Assembly for Dynamic Calibration of Water Current Meters.

Figure 2

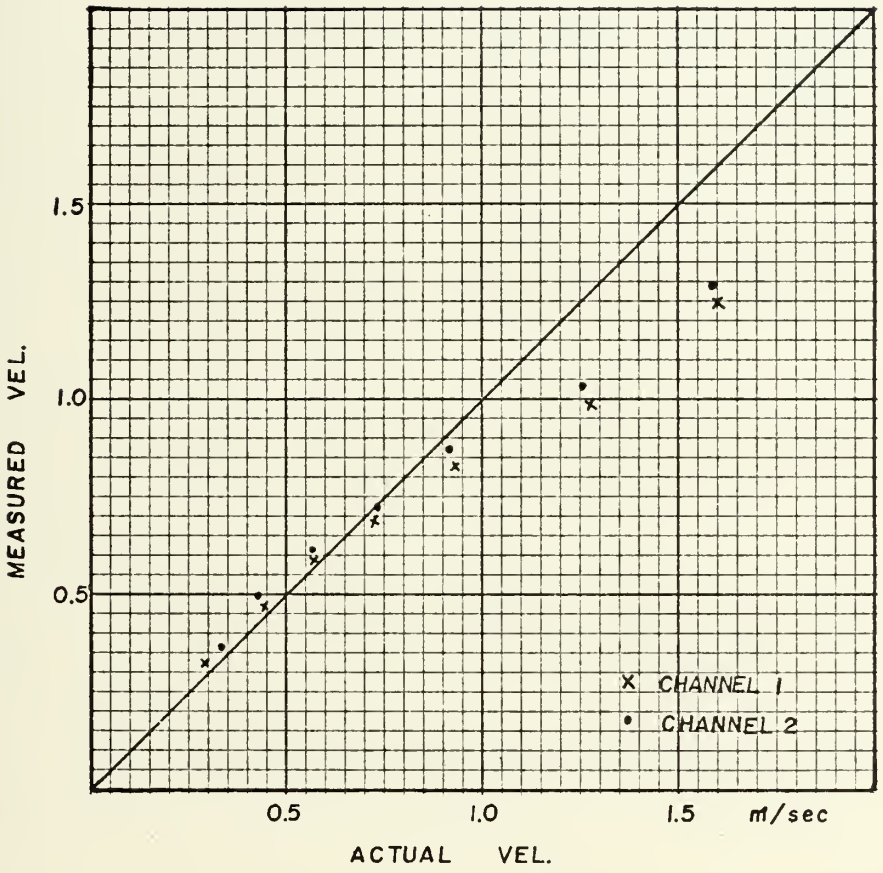

Measured and Actual Velocities. Current Meter Serial Number 637 (Used at 69 cm Depth)

Figure 3

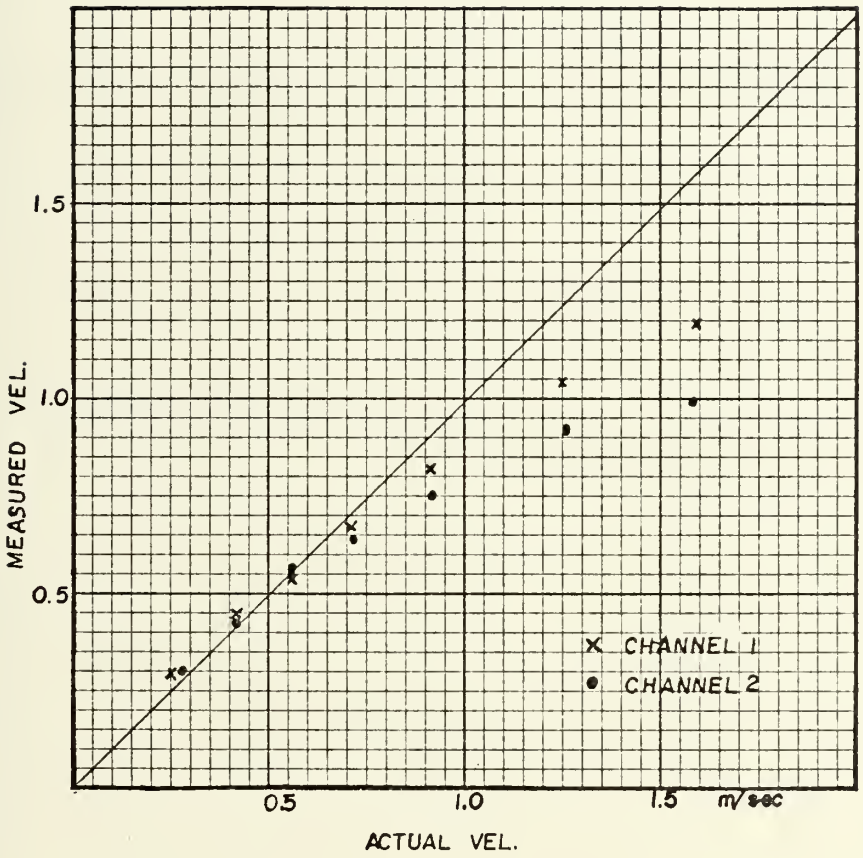

Measured and Actual Velocities. Current Meter Serial Number 638. (Used at 39 cm Depth)

Figure 4

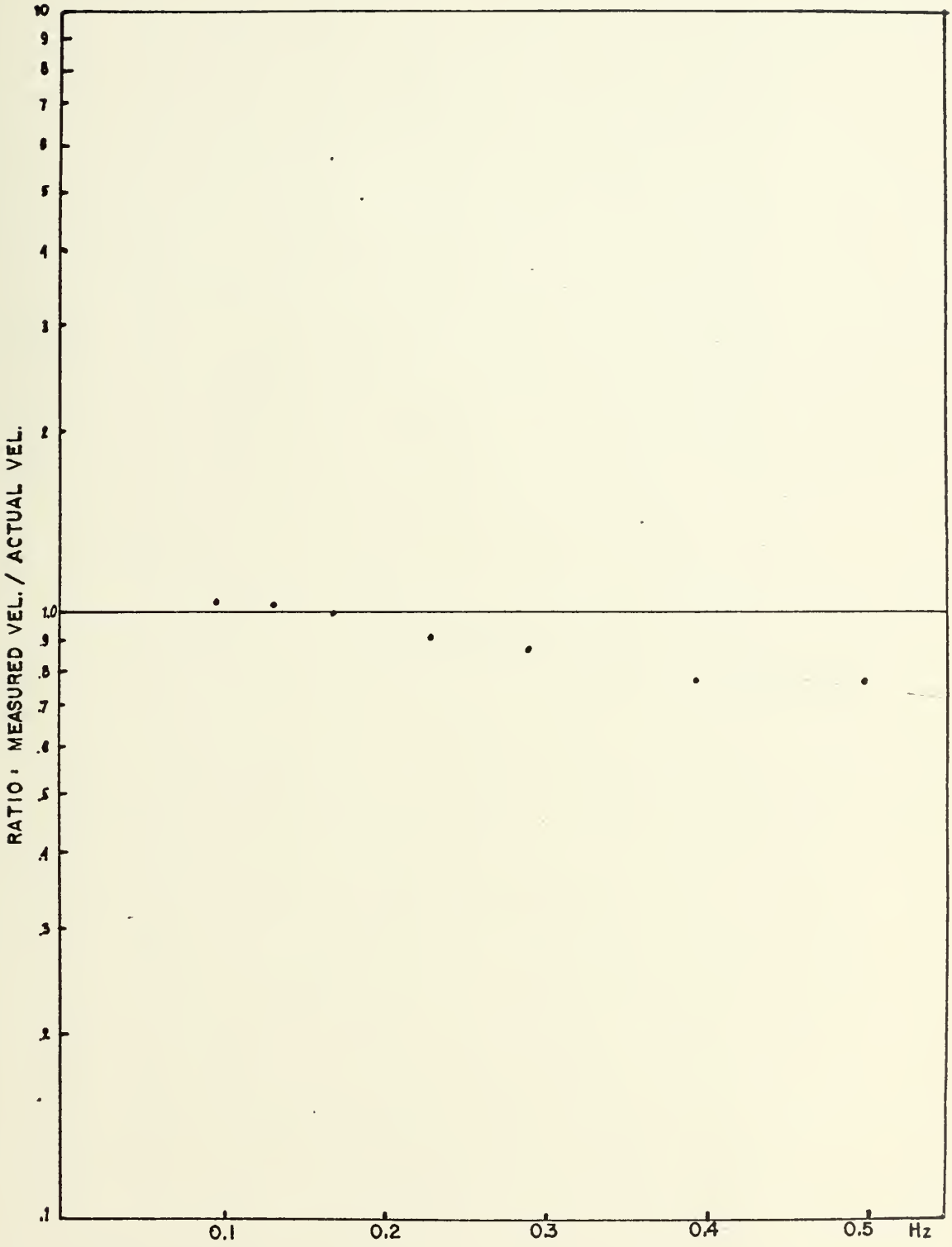

Frequency Response of Water Current Meter
Serial Number 637

Figure 5

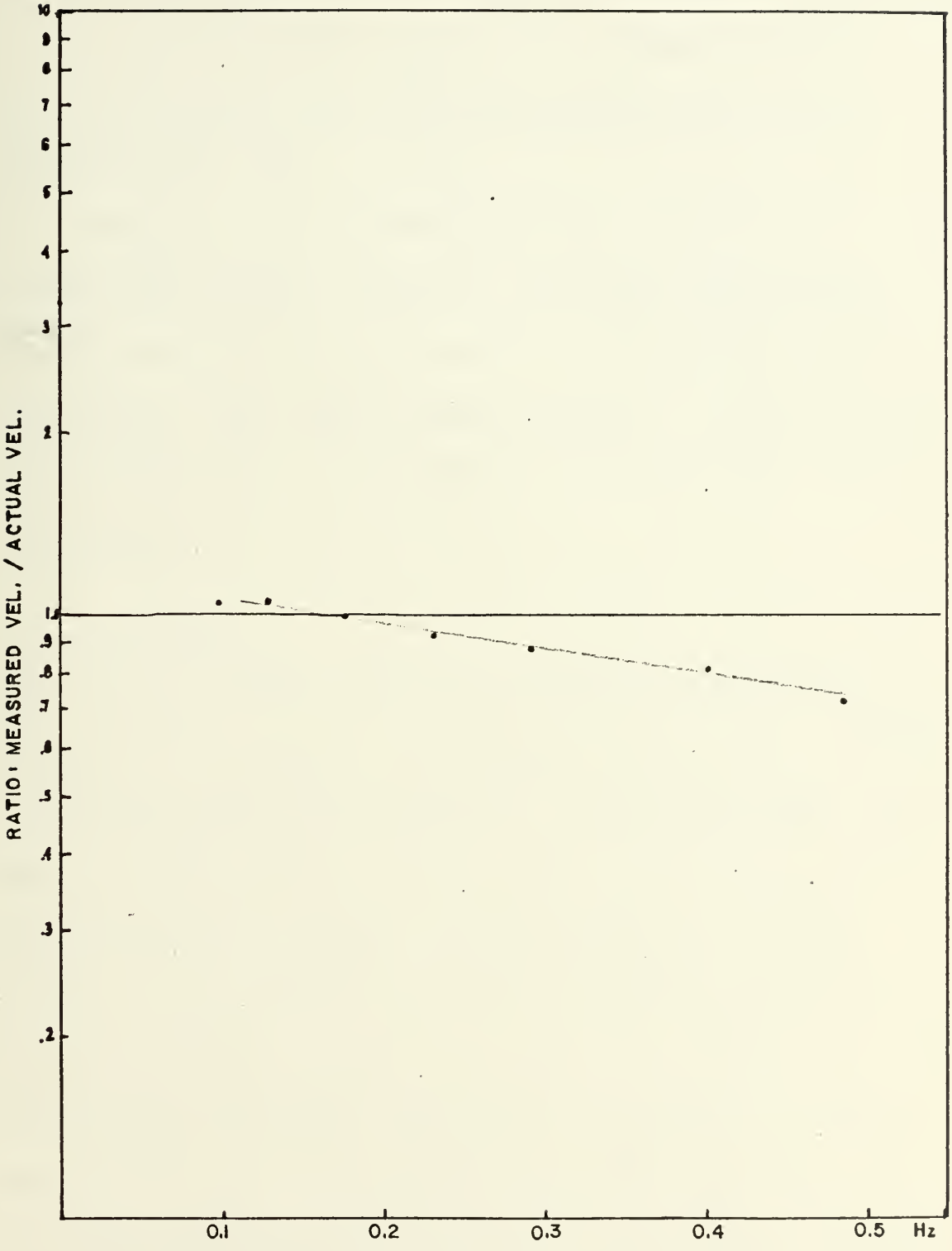

Frequency Respone of Water Current Meter
Serial Number 638.

Figure 6

corresponds to the time required for the signal to decrease by 3 db from the true value, that is, when $V_m/V_t = 0.707$. Referring to Figures 5 and 6, the instruments have an average response time of 2 seconds corresponding to 0.5 Hz.

The probe is made of fiberglass material with dimensions 11 inches in length and 3/4 inches in diameter. The system senses variations in velocities over an area of approximately two to three probe radii from the transducer. This limits the spatial resolution to disturbances with a wave length of 11 cm, corresponding to a deep water wave period of 0.27 seconds.

B. WAVE GAGE

The water surface elevation was measured with an Interstate Electronics Corporation SDP 201 differential pressure sensor, and a DP 200 wave recorder, shown in Figure 7. The pressure sensor is a small, unbonded strain gauge bridge. Direct current exitation for the bridge is supplied by a voltage regulator located in the transducer housing. The sea pressure is coupled by a neoprene diaphragm to a silicone fluid filling the interior. One part of the transducer is exposed directly to the interior fluid, and the other is connected to a chamber which is connected to the interior fluid by a length of capillary tubing.

This arrangement acts as a hydraulic filter developing a reference pressure which is an average value of the external sea pressure. By the action of this filter, the transducer senses rapid pressure fluctuations only and slow changes such as tides are lost through the hydraulic filter.

The dc signal voltage output has a range of $\pm$ 2.5 volts. In the wave recorder, the signal is transferred to a chart paper. The recorder also has an outlet for an external recording system. Maximum dynamic range of the wave meter is $\pm$ 20 feet with a linearity of one percent.

In addition, a stilling well type mean water level indicator was used. This was a two inch diameter clear plastic tubing capped on both ends with a 1/16 inch diameter hole in the bottom and a 3/8 inch hole in the top for an air vent. The mean water level was measured by viewing the water level using a surveyor's transit from the shore and comparing it to a graduation on the side of the tubing.

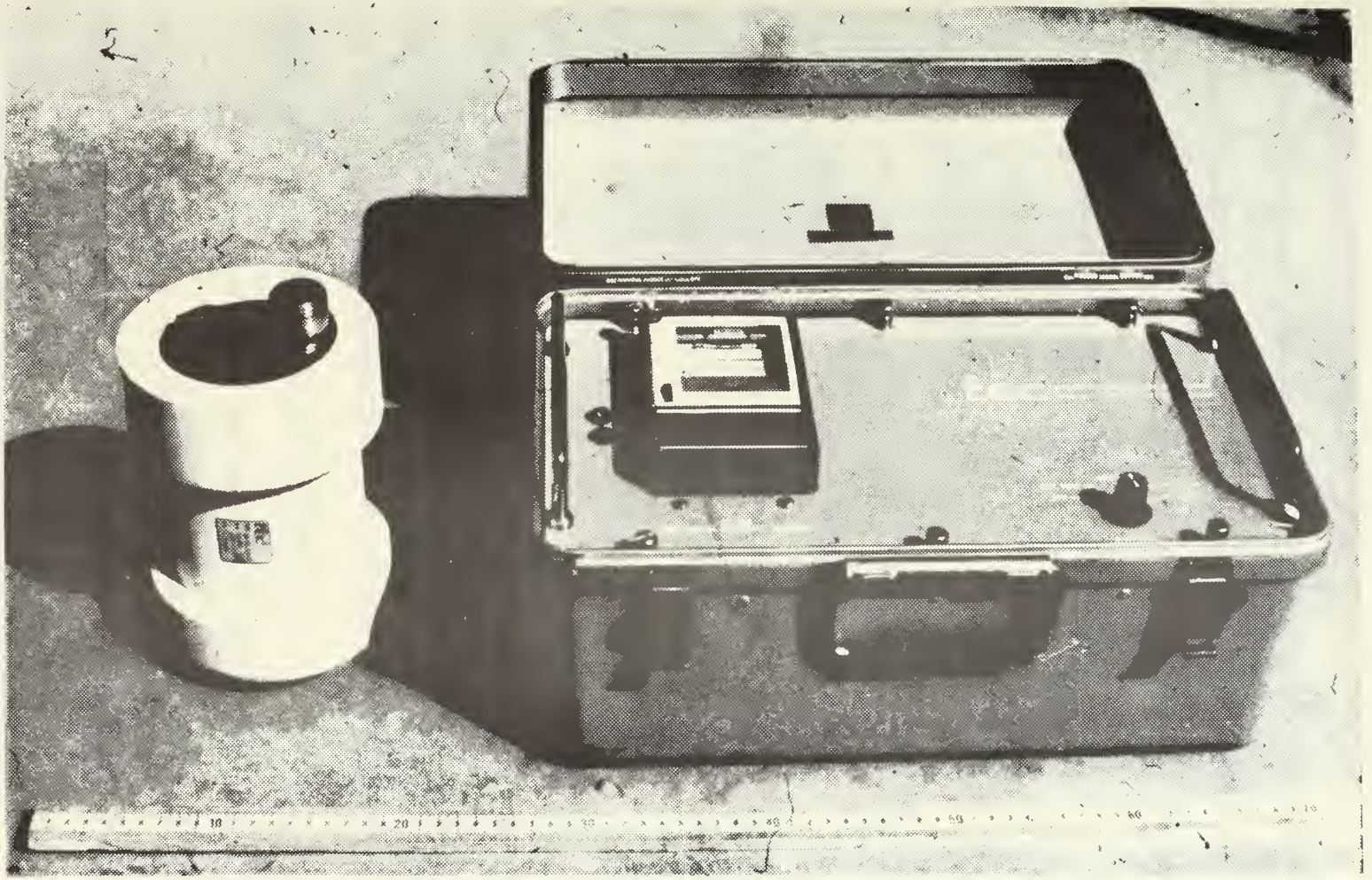

IEC DP200 Portable Wave Recorder and SDP201 Wave Gage.

Figure 7

IV. PRESENTATION OF DATA

A. MEASUREMENT TECHNIQUES

The experiments were performed at Del Monte Beach in front of the Naval Postgraduate School beach laboratory, on August 1, 1972. The waves at this location are generally highly refracted and directionally filtered, and break almost parallel to the shore line. At the time of making the measurements the breaking waves generally were of the spilling type with an occasional plunging type.

It is necessary to mount the instruments on a stable platform that does not vibrate and can stand the forces of the breaking waves. A tower was built for this purpose and arranged as shown schematically in Figure 8. The tower was constructed of 2 inch diameter steel pipe with a two foot diameter flat circular base to keep it from sinking into the sand. It was fastened to the ground by four stays tied to screw-type anchors buried approximately 2 feet in the sand. The tower was tested for endurance before the actual taking of data for a period of 24 hours. The entire structure proved to be very stable; the vibration was very small and was neglected in the calculations.

The transducers were arranged such that they were aligned vertically in order to get measurements in the same column of water. The two flow meters were oriented to measure vertical and horizontal (inshore-offshore) water particle velocities. They were mounted at the end of a horizontal 3/4 inch diameter pipe that extended approximately

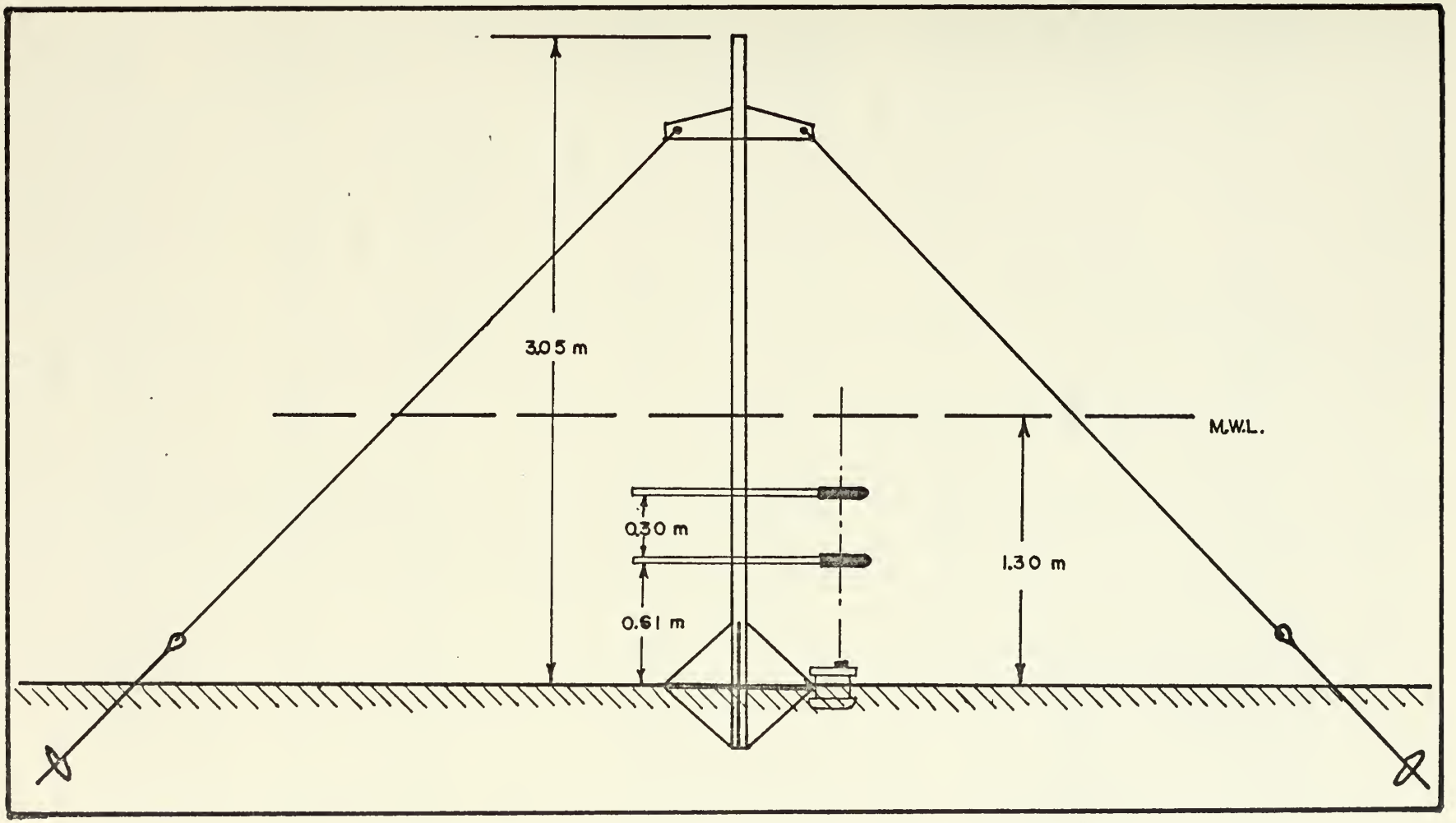

Schematics of Tower Used in Taking the Measurements Showing the Location of The Instruments.

Figure 8

equal lengths to both sides of the tower; this was for the purpose of minimizing any torque caused by the forces of the waves that might cause movement or vibrations of the probes. The wave gage was fastened to the base of the tower directly below the flow meter transducers.

Figure 9 is a picture of the tower, with instruments mounted on it, at low tide. Measurements were made at high tide. Instruments were placed and recovered at low tide. Figure 10 shows the beach profile with the location of the tower, still water level, and the approximate wave breaking point at the time of recording data.

Measurements include four velocity records (horizontal and vertical for each of two current meters), sea surface elevation in the same column of water, and the sea surface elevation approximately 800 m offshore. A record of 15 minutes from the total recorded data was chosen for analysis. This record was taken 1 August 1972 commencing at 1705. The mean depth of water during the run was 1.3 meters.

B. DATA PRE-PROCESSING

The data was simultaneously recorded using a Sangamo Model 3500, 14 channels FM magnetic tape recorder. The information being recorded was monitored continuously with a strip chart recorder and a volt-meter.

The data was transcribed to an eight channel Clevit Brush strip chart recorder for verification using the CS-500 analog computer, and digitized and recorded onto a 7-track tape using an XDS-9300 computer.

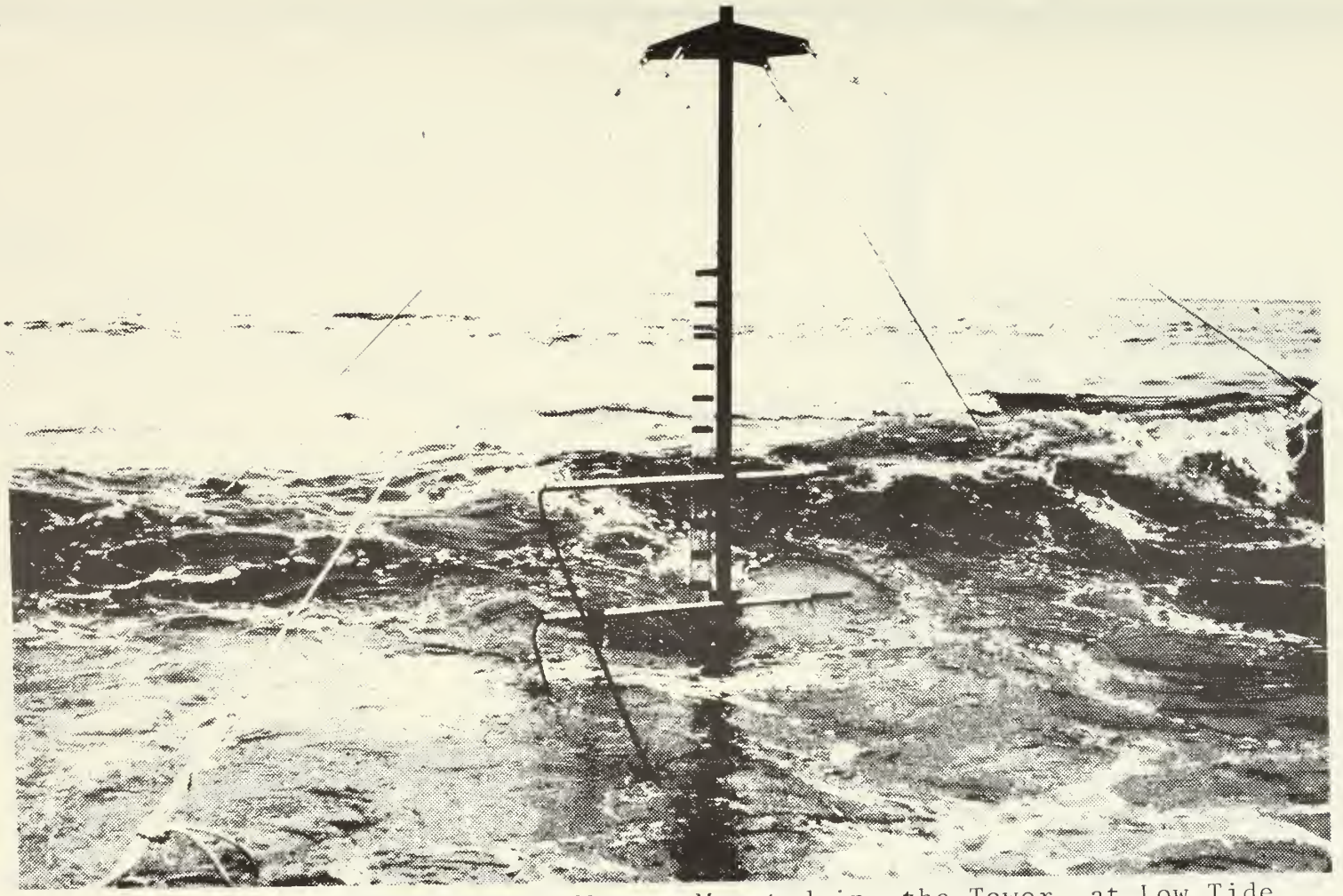

Water Current Meters Mounted in the Tower, at Low Tide.

Figure 9

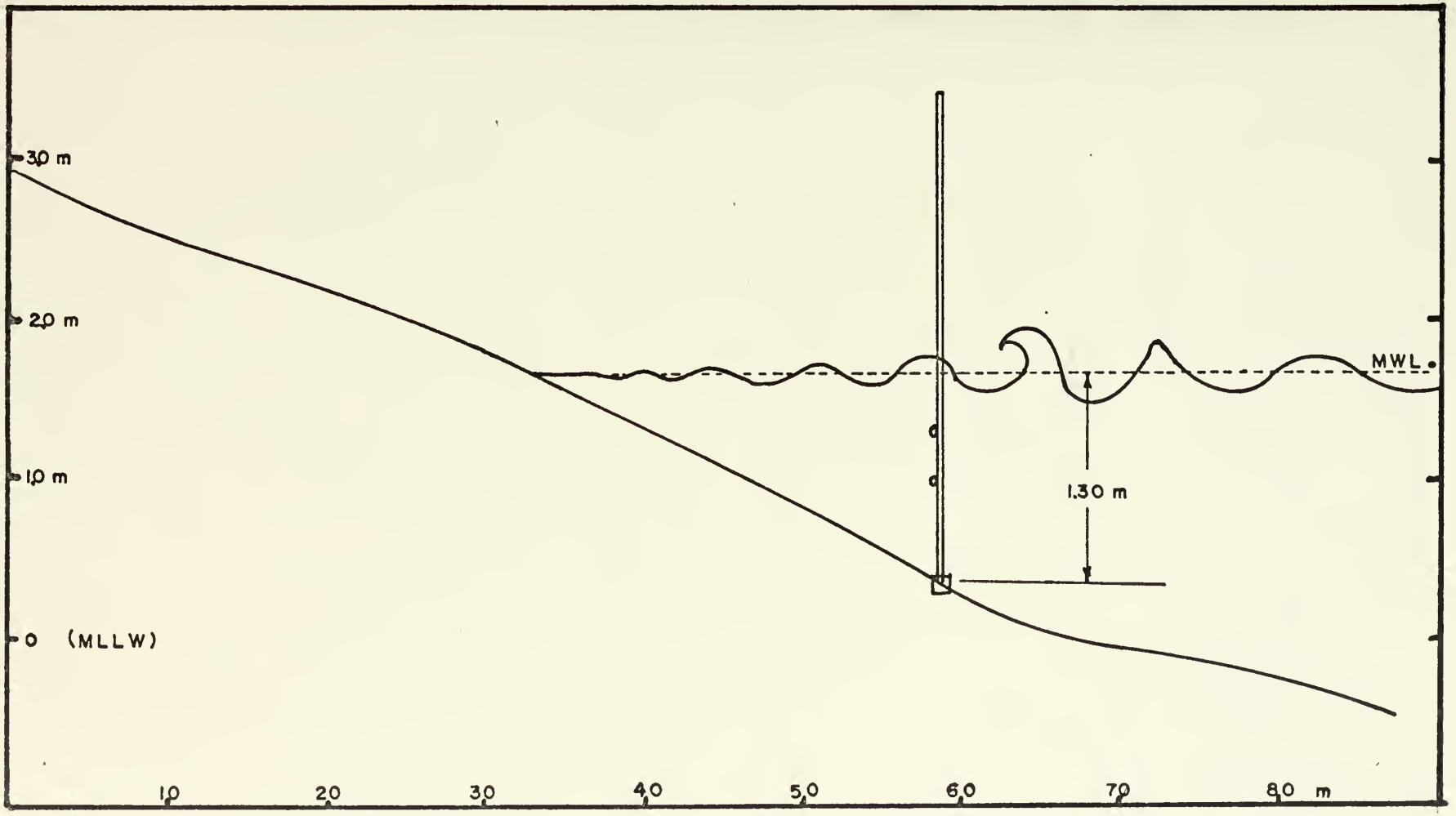

Beach Profile with Location of Measurements Site.

Figure 10

A sample of the records from one of the flow meters and from the two wave recorders is shown in Figure 11. Digitization was made at a rate of 10 samples per second, corresponding to a sampling interval of 0.1 second. The digitized records were transferred to a data cell in the IBM 360 computer for analysis.

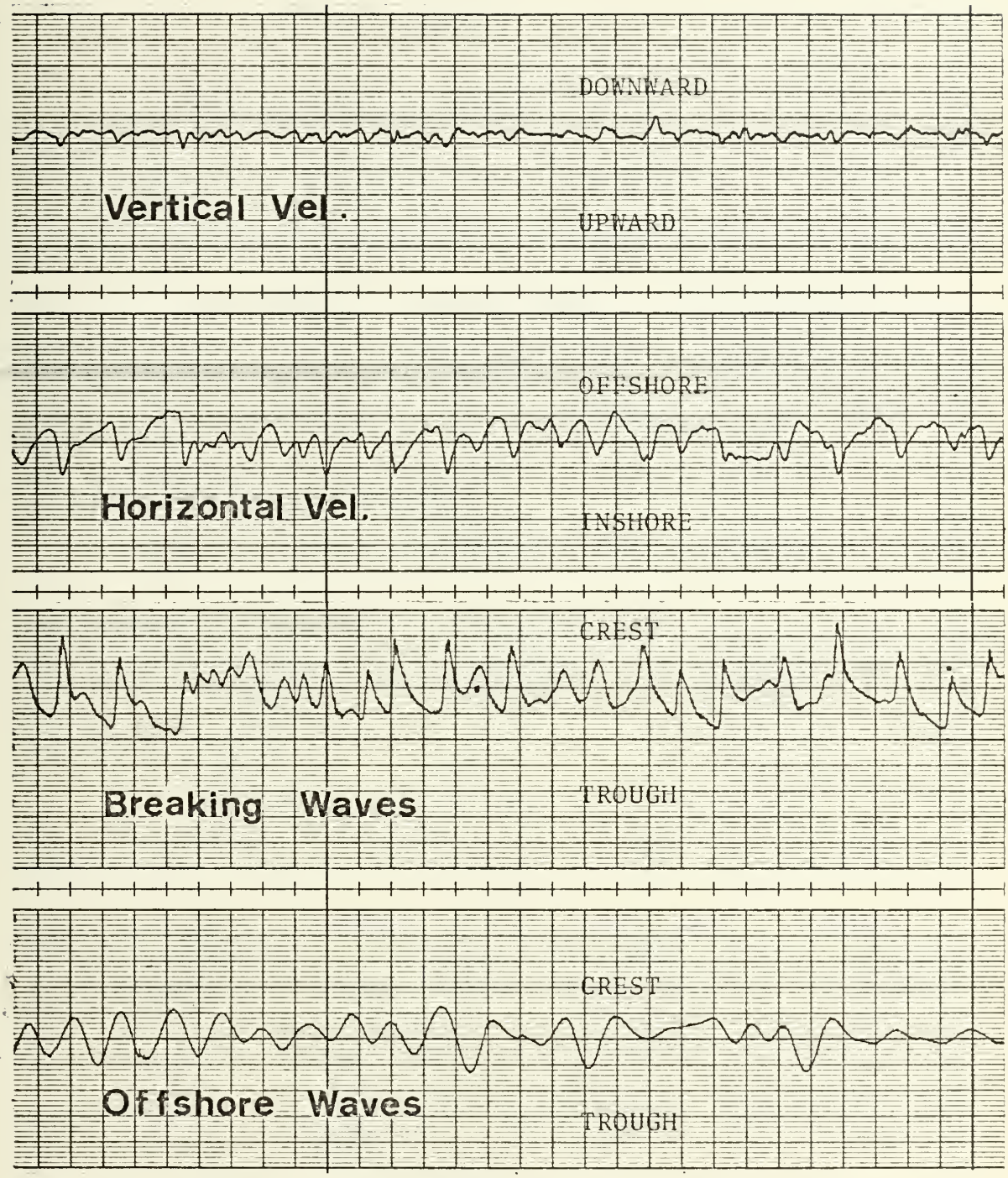

Strip Chart Record Sample

Figure 11

V. ANALYSIS

A. PROBABILITY DENSITY FUNCTIONS

The probability density functions for each of the time series was calculated and plotted. Comparison was made with a standard Gaussian distribution. The variance, standard deviation, and skewness of the distributions were determined. The curves were normalized (units on the horizontal axis are measures of standard deviation, s).

1. Sea Surface Elevation

The pdf for the offshore wave record matches fairly well the normal distribution (Figure 12). This agrees with theory in that the sea surface elevation in relatively deep water can be approximated by a Gaussian distribution.

On the other hand, the breaking wave pdf (Figure 13) was found to be positively skewed (skewness = 0.58). This means that positive values are larger but less frequent than negative values which are more frequent but smaller. In other words, the crests are steeper and more peaked, whereas the troughs are elongated and flatter. A schematic of such a surface is shown in Figure 14. This is how waves in shallow water theoretically appear.

2. Vertical and Horizontal Water Particle Velocities

In relatively deep water the horizontal and vertical water particle velocities induced by wave motion are approximately equal for positive and negative directions. However, as the waves move into

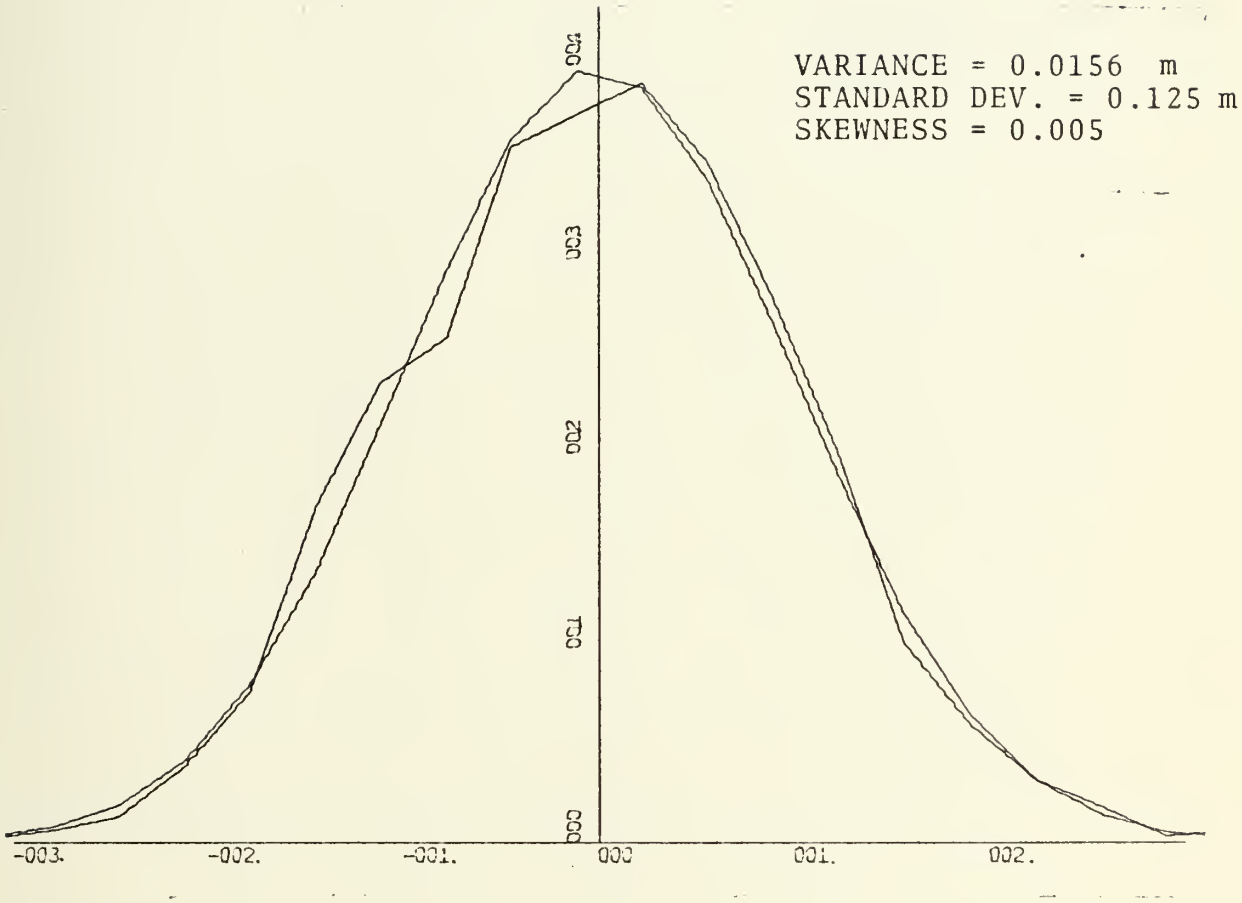

Probability Density Function of Sea Surface Elevation Outside Surf Zone.

Figure 12

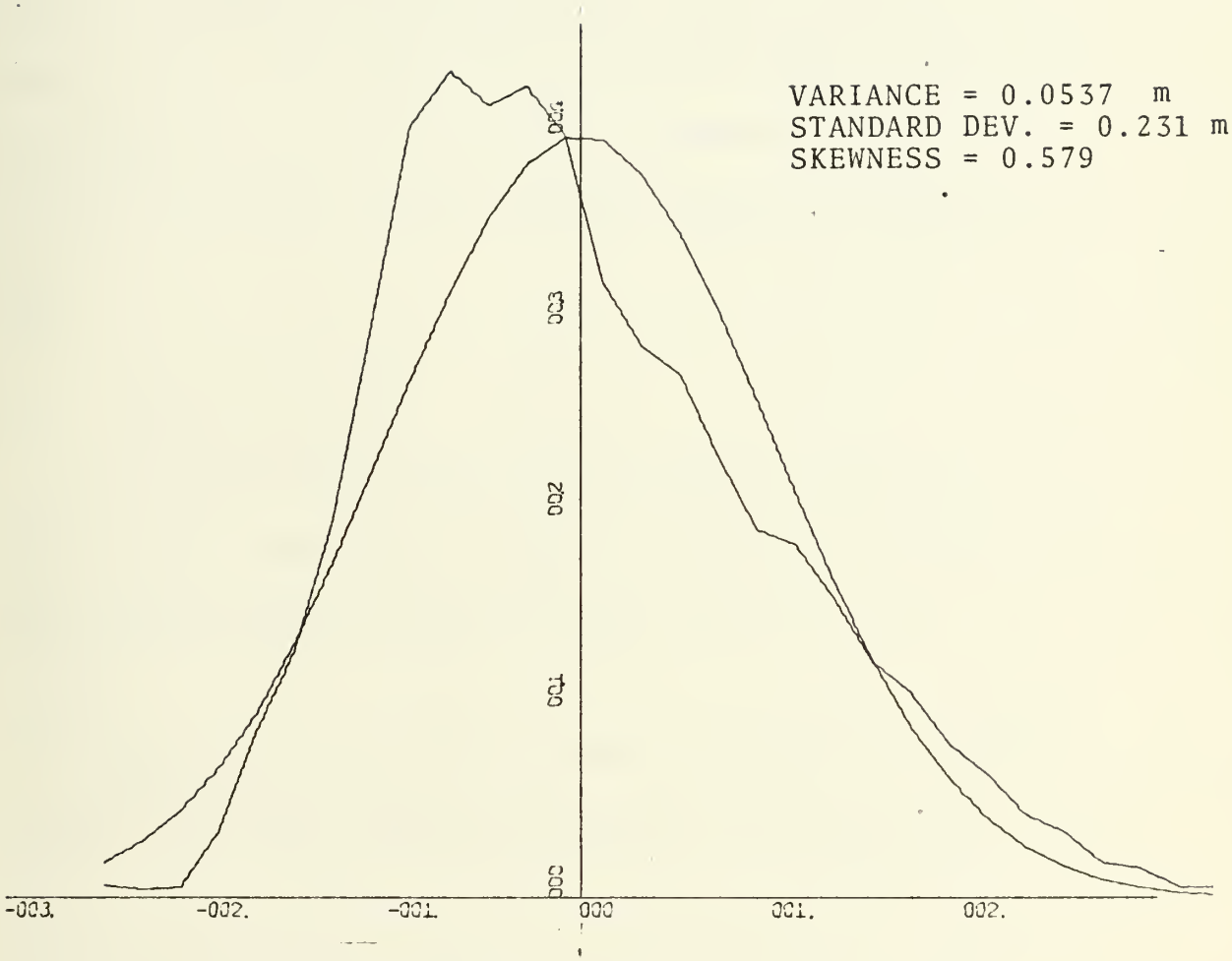

Probability Density Function of Sea Surface Elevation Inside Surf Zone.

Figure 13

shallower water they become asymmetrical and induce asymmetry in the velocity of the water particles, the inshore and upward velocities being greater in magnitude and of shorter duration than the offshore and downward velocities. This asymmetry is found in the water particle motion inside the surf zone and is shown by the skewness of the pdf of the horizontal and vertical particle velocities respectively (Figures 15 and 16).

B. SPECTRAL ANALYSIS

The energy-density spectra were calculated for each variable and cross-spectra computed for each pair of variables inside the surf zone. Cross-spectral analysis was also made for the offshore and inshore wave records.

The initial sampling of the records was made at a 0.1 second interval. However, every other sample was taken in making the computations giving an actual sampling interval of 0.2 second and a niquist frequency of 2.5 hertz. Testing showed this to be a sufficiently high sample rate to avoid aliasing in the spectra. The maximum time lag was chosen to be 10 percent of the record length and the length of record analyzed was 15 minutes. This results in a band width resolution of 0.0057 hertz and each spectral estimate having 20 degrees of freedom.

1. Offshore and Inshore Sea Surface Elevation

The offshore and inshore sea surface elevations were measured using pressure wave gauges. In order to represent the pressure

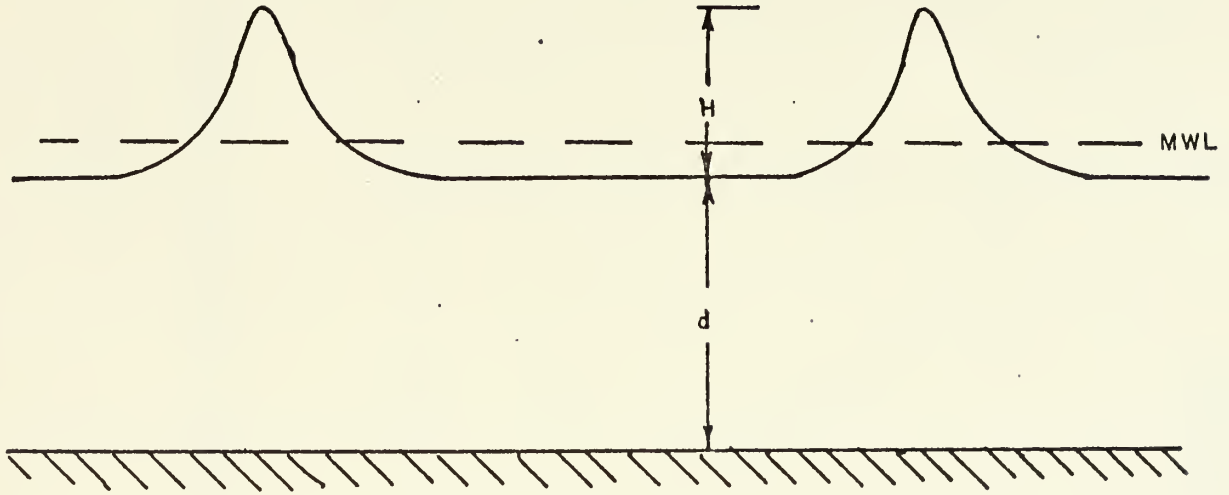

Schematic of Sea Surface with Peaked Crests and Elongated Troughs

Figure 14

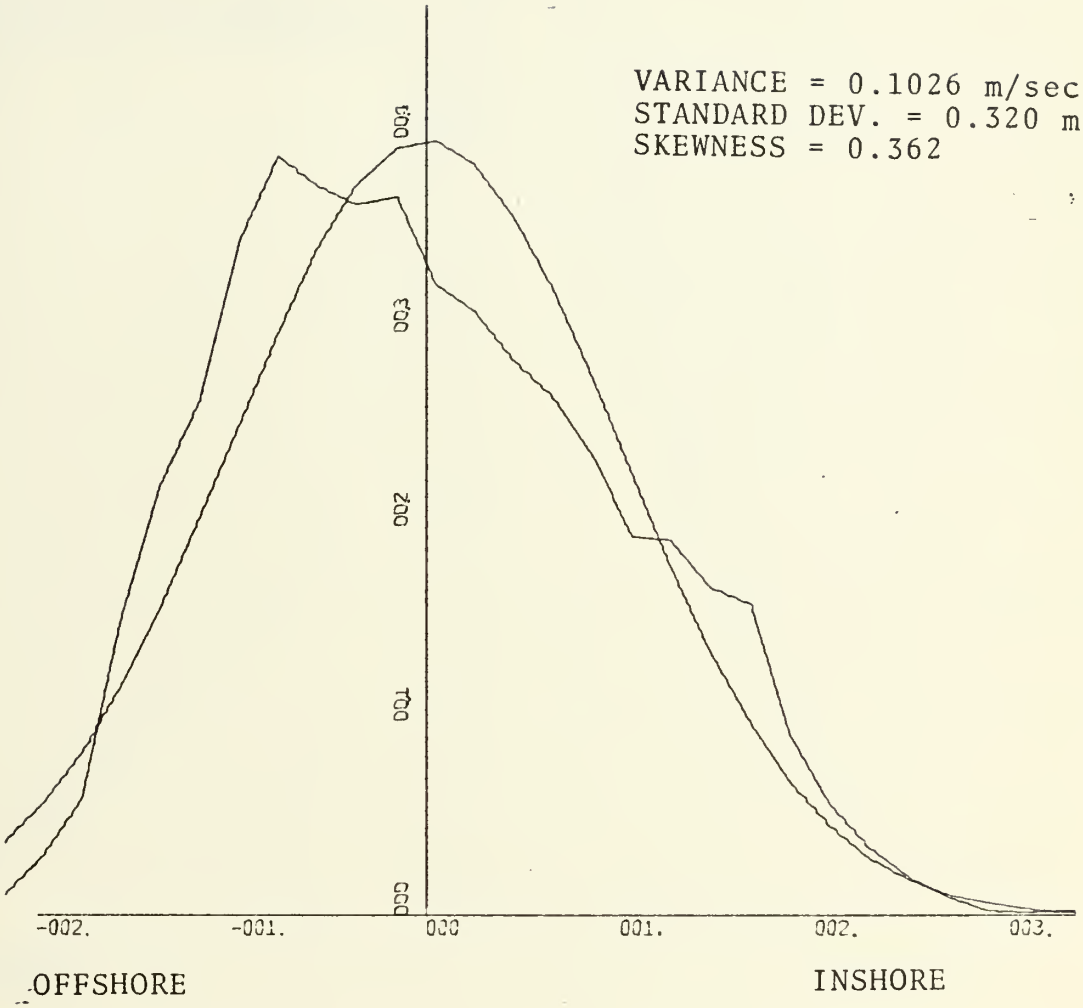

Probability Density Function of Horizontal Water Particle Velocity Inside Surf Zone.

Figure 15

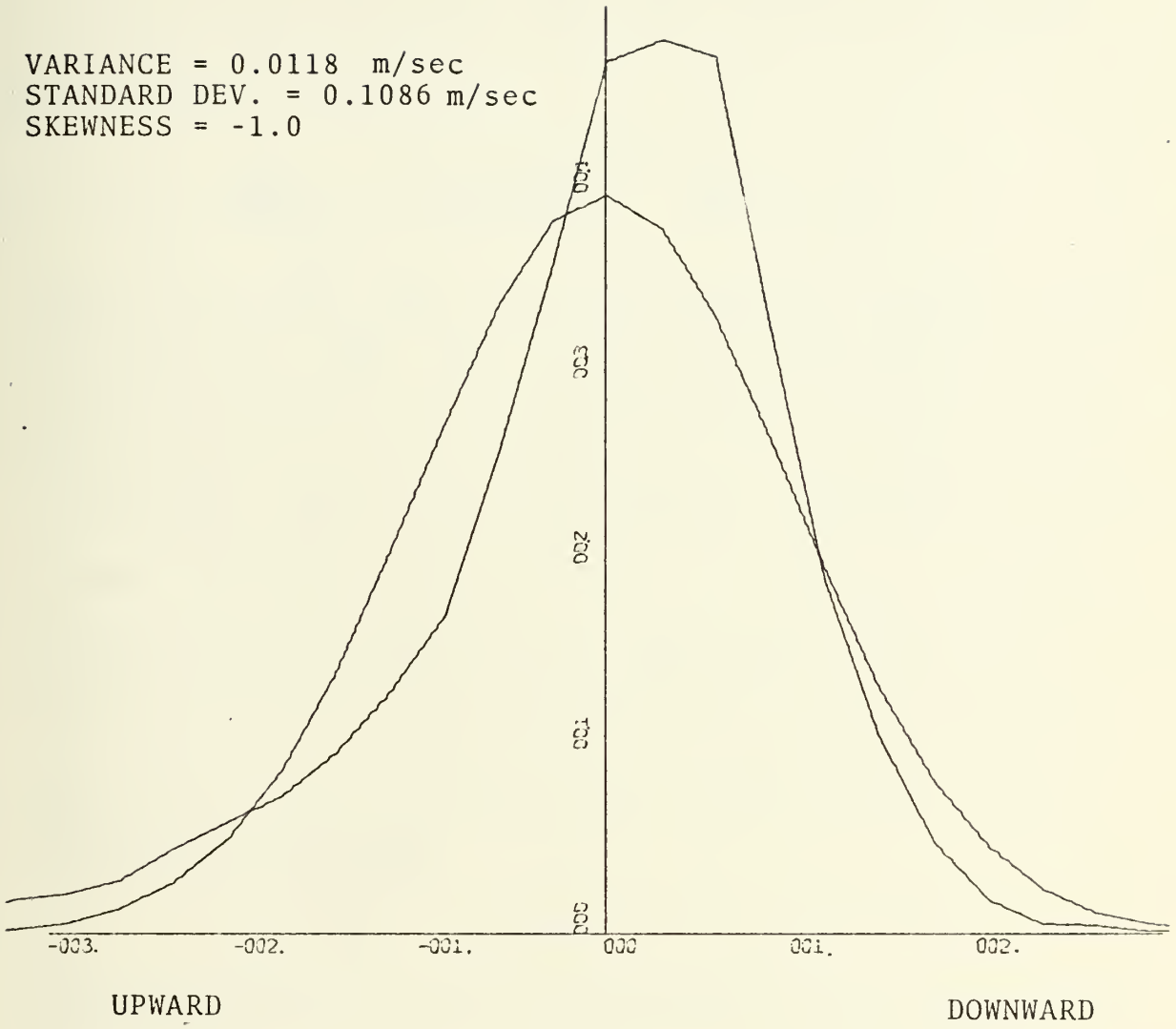

Probability Density Function of Vertical Water Particle Velocity Inside Surf Zone.

Figure 16

records as measures of the sea surface elevation a correction factor was applied to the pressure spectra. This factor is based on linear theory and is given by the expression

$$\Phi_{\text{wave}}(f) = \left[\frac{\cosh k(h - x)}{\cosh kh}\right]^2 \Phi_{\text{pressure}}(f)$$

where h is the bottom depth, x is the wave gauge sensor depth, k is the wave number, and $\Phi(f)$ represents the energy-density spectra. A maximum limit of 100 was established for this correction factor as applied to the spectra. This cut-off is represented by a sudden drop in the spectra at higher frequencies (Figure 17). The correction factor is not applied to the wave spectrum in Figure 17 for the region inside the surf zone. In subsequent figures the correction factor has been applied to the waves inside the surf zone, although the validity of linear theory is highly questionable in this region.

The offshore wave energy-density spectra show a maximum peak at a frequency of 0.19 Hz, corresponding to a wave period of 5.25 seconds. Inside the surf zone there is a peak at about this same frequency although the magnitude is smaller. Other peaks are present at frequencies corresponding to one-half and one-third of 0.19 Hz. These peaks might be caused mainly by the shoaling of the offshore waves. However, some kind of non-linear interaction might also be present as there is an increase in the magnitude of the spectra in some of the harmonic and sub-harmonics of the basic frequency.

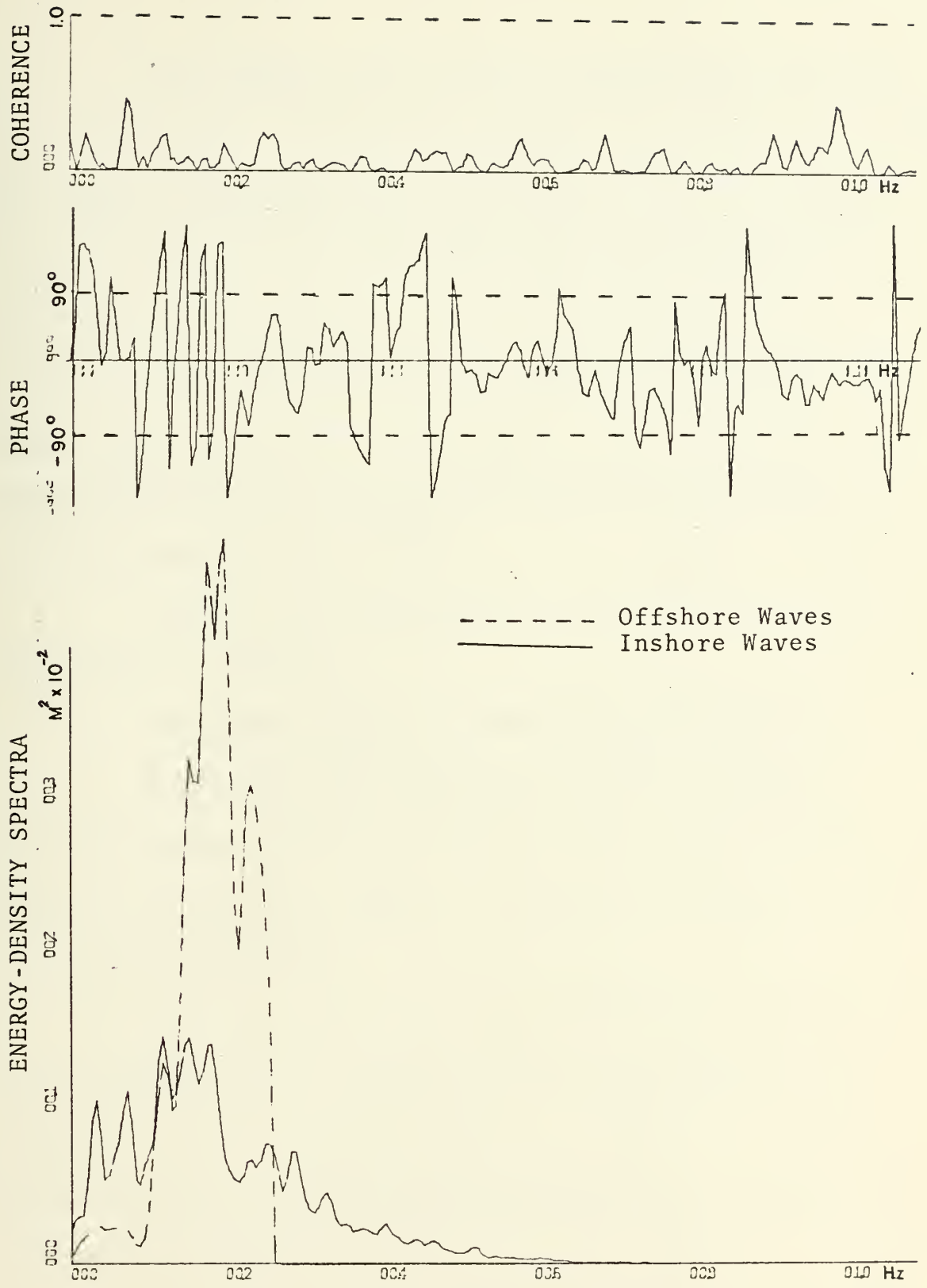

Spectra of Sea Surface Elevation Offshore and Inside Breaking Zone.

Figure 17

There appears to be a decrease of energy-density inside the surf zone compared to offshore in the frequency band of about 0.1 - 0.2 Hz. This decrease is apparently due to the breaking of the waves; although the energy-density levels for the offshore waves are questionable at frequencies higher than about 0.1 Hz due to the increasingly larger correction factor. There appears to be a shifting of energy-density to higher frequencies for the waves inside the surf zone. An increase would be expected at frequencies higher than the wave band due to turbulence generated during breaking.

The two wave records show no relationship to each other in phase angle nor coherence.

2. Sea Surface Elevation and Water Particle Velocities

According to wave theory the wave induced horizontal velocity is in-phase with the sea surface elevation, and the vertical velocity is 90 degrees out of phase with both the sea surface elevation and the horizontal velocity.

The cross-spectra of sea surface elevation with each one of the horizontal particle velocities at 39 and 69 cm depth were very similar as that shown in Figures 18 and 19. The same is true for the cross-spectra of sea surface elevation with the vertical velocities at the two depths (Figures 20 and 21).

a. Horizontal Particle Velocities

The results show a very good coherence for each of the horizontal velocities in relation to the sea surface elevation in the

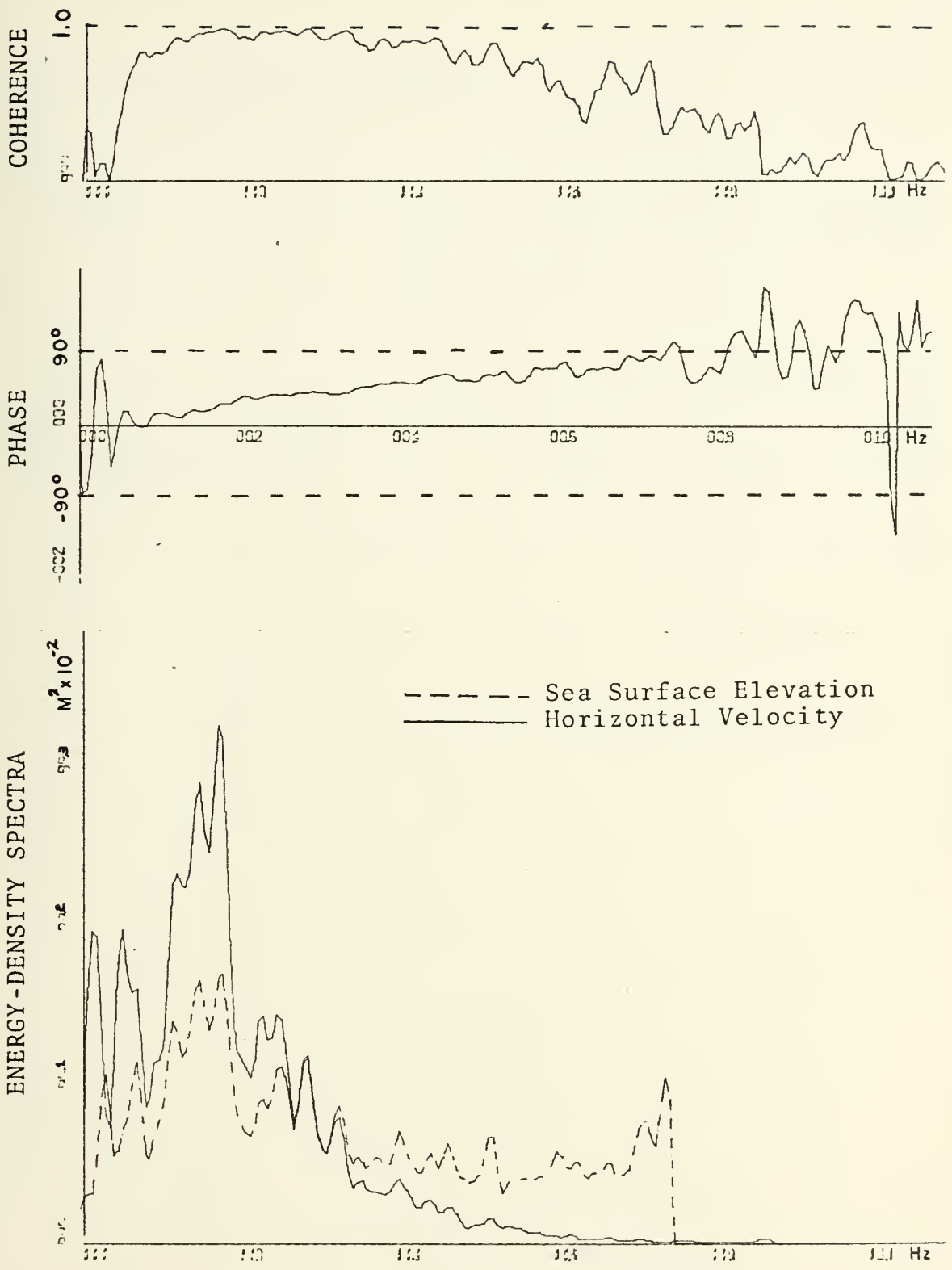

Spectra of Sea Surface Elevation and Horizontal Particle Velocity, Depth 39 cm.

Figure 18

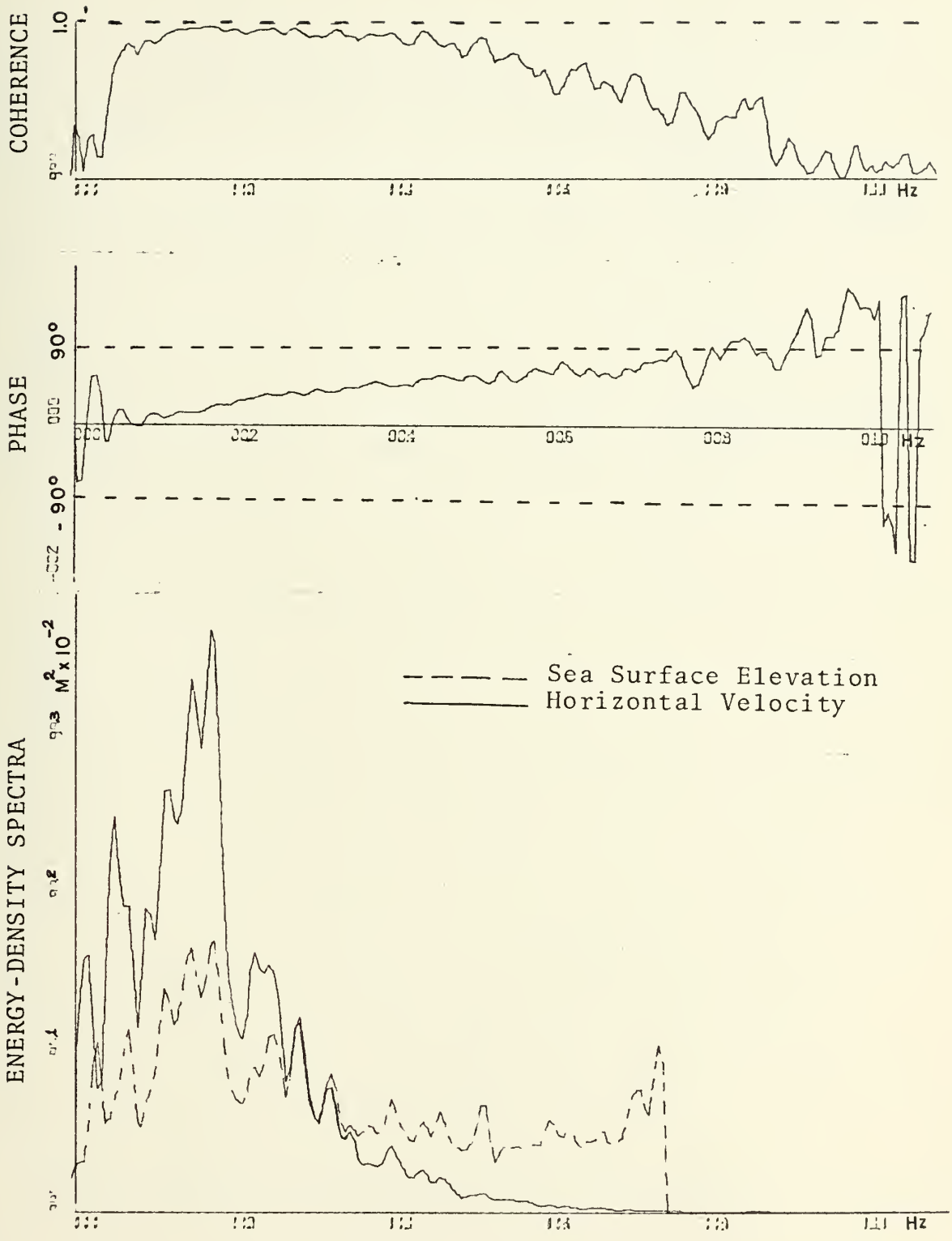

Spectra of Sea Surface Elevation and Horizontal Particle Velocity, Depth 69 cm.

Figure 19

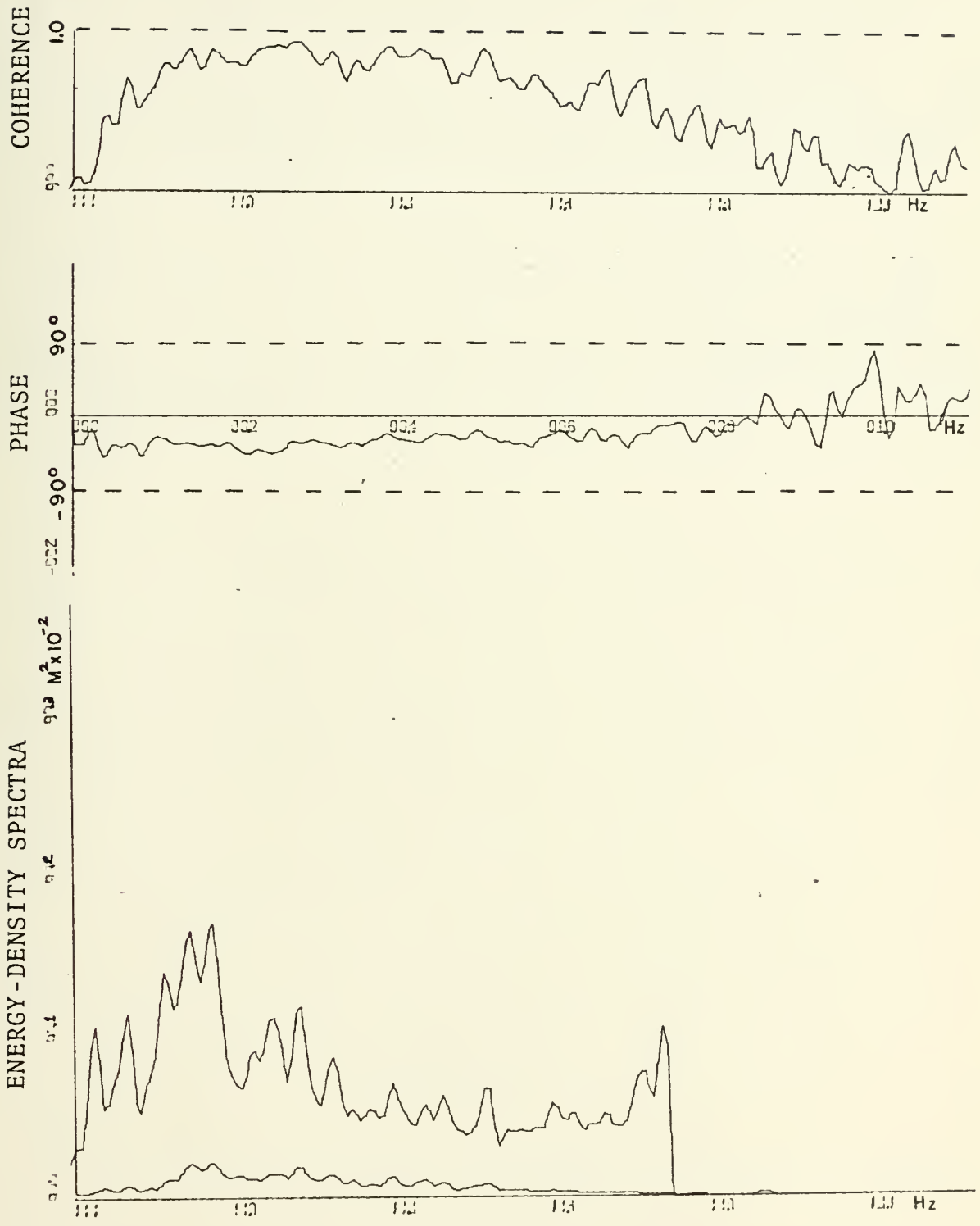

Spectra of Sea Surface Elevation and Vertical Particle Velocity, Depth 39 cm.

Figure 20

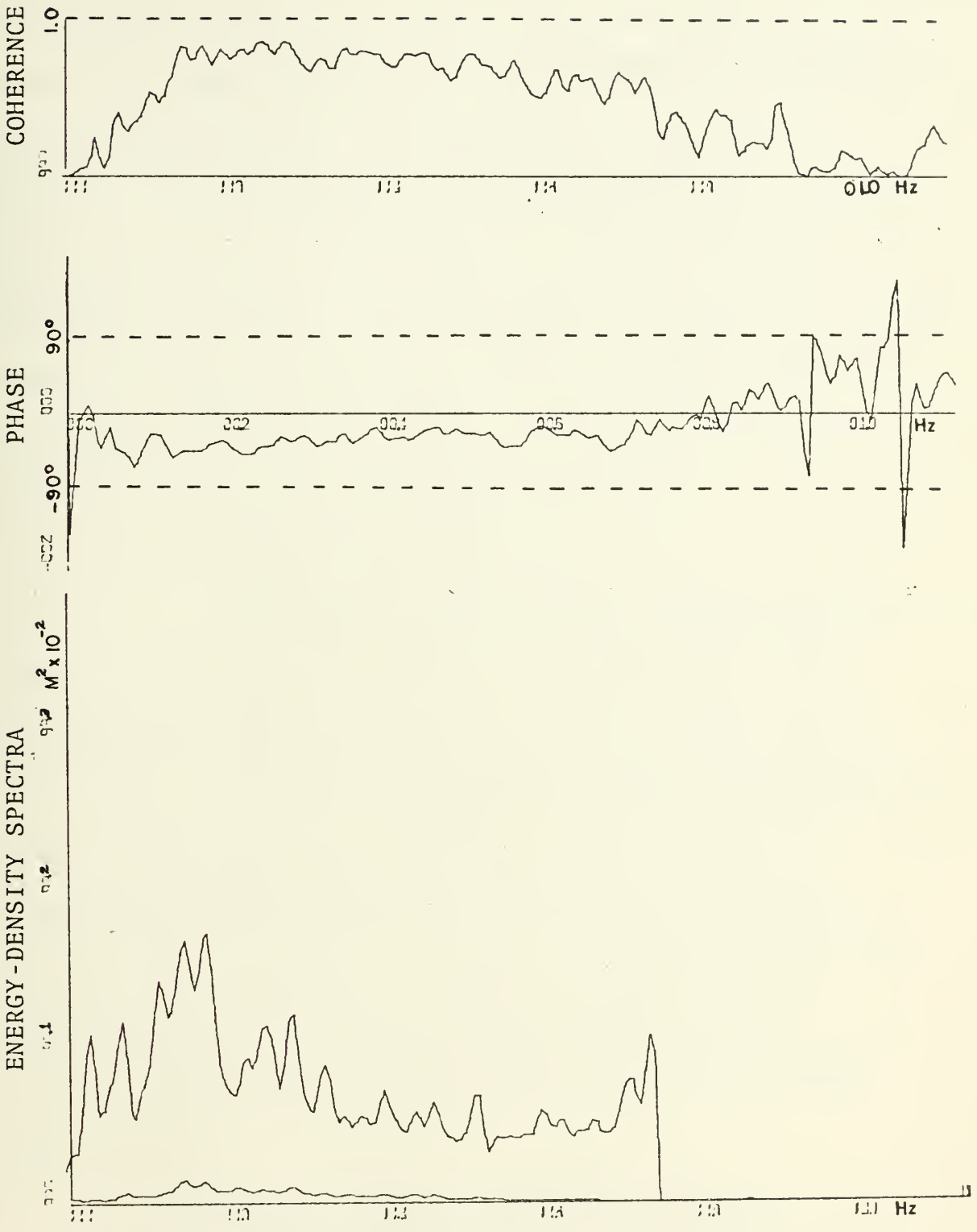

Spectra of Sea Surface Elevation and Vertical Particle Velocity , Depth 69 cm.

Figure 21

range of frequencies where most of the energy is concentrated. The coherence in this range reaches a value of over 0.9 and starts decreasing after approximately 0.7 Hz. This is probably due to the increase in turbulence in higher frequencies and the general decrease in energy level. The phase angle shows a shift as frequency increases in the well-correlated zone of the spectrum. At low frequencies it has a value of 0 degrees, agreeing with linear wave theory, but increases steadily up to 90 degrees phase angle in the frequencies of 0.7 Hz. The phase angle becomes unstable for the non-coherent region of the spectrum.

b. Vertical Particle Velocities

The spectral analysis of vertical velocities and sea surface elevation give slightly lower coherence values than for the horizontal velocities, but it is still over 0.75 for the range of high energy of the spectra. The phase angle in this case is less than the theoretically predicted values using linear wave theory. There is no noticeable shifting in phase except for frequencies higher than 0.8 Hz, where it begins to fluctuate, again probably due to turbulence. The area under the energy-density spectra is considerably less than that for the horizontal velocities. This indicates that the kinetic energy due to vertical particle velocity is small.

3. Horizontal and Vertical Water Particle Velocities

The cross-spectra between the two horizontal velocities and the two vertical velocities at the 39 cm and 69 cm depths were calculated with the intent of finding the relation between these parameters

and the distribution of kinetic energy at two different elevations in the water column. The two horizontal particle velocities show a very good coherence and 0 degrees phase angle within the significant range of the spectrum (Figure 22). The energy-density spectra have the same shape for both depths but the one calculated at depth of 69 cm has greater energy-density. This indicates that the kinetic energy at the shallower depth was smaller than at the intermediate depth. This result was not expected since the horizontal particle velocities according to wave theory are highest at the surface and decrease with depth. It is possible that there is a different vertical distribution of velocities after the breaking of the wave, but more studies are necessary in order to make any conclusions.

In the analysis of vertical velocities shown in Figure 23, a good coherence and 0 degrees angle of phase is also found between the two records in the significant energy-distribution range. The area under both spectra (which is proportional to the kinetic energy due to vertical velocities) is very small. The spectrum corresponding to the shallower depth is larger than the deeper one, as expected, considering that the vertical velocities at the bottom must be zero (if percolation is not considered).

The spectral analysis for horizontal and vertical velocity pairs are shown in Figures 24 and 25. The results look very similar for both depths. The coherence oscillates between 0.7 and 0.9 in the region of maximum energy. The phase angle oscillates about the value

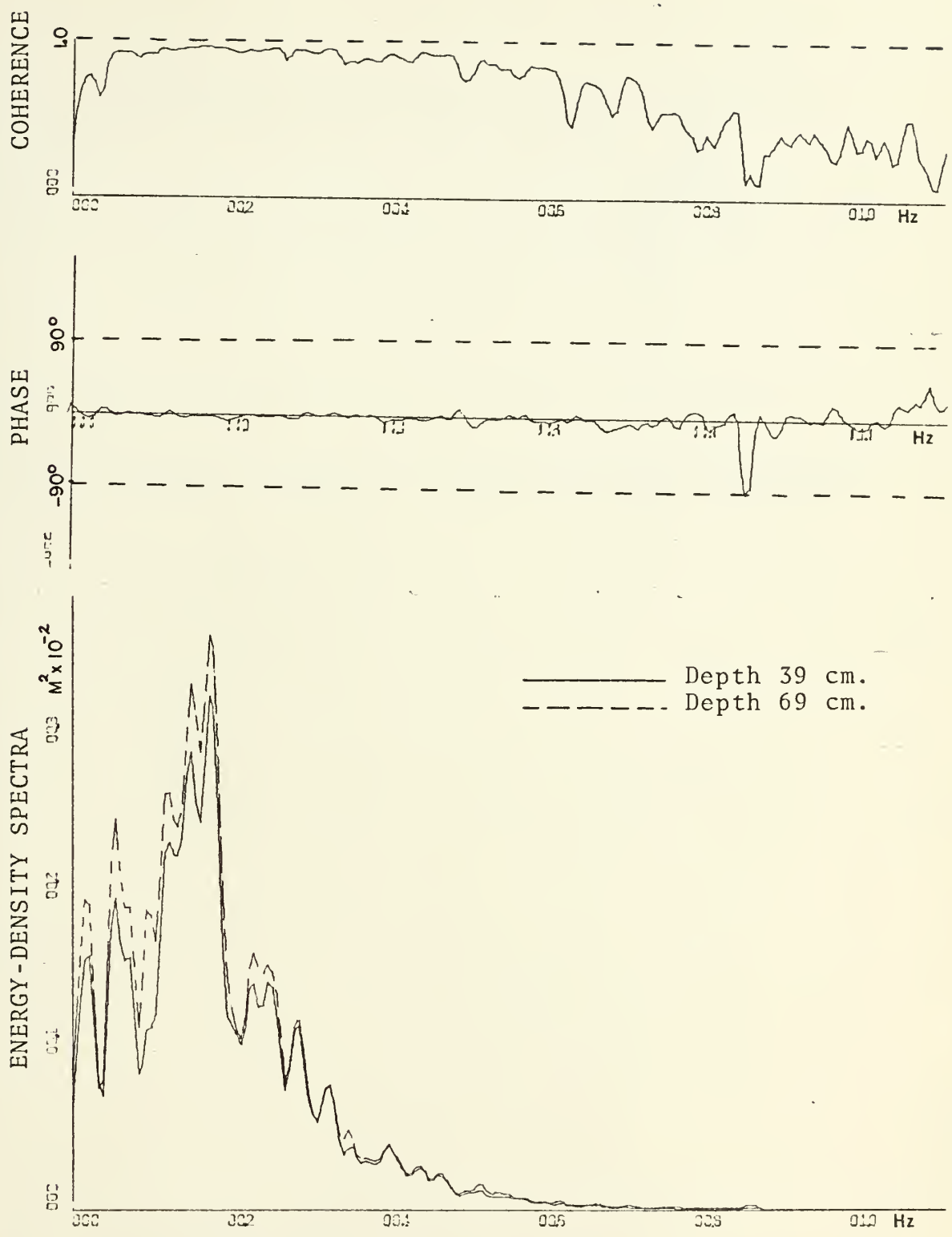

Spectra of Horizontal Particle Velocity at Depth 39 cm and Horizontal Particle Velocity at Depth 69 cm.

Figure 22

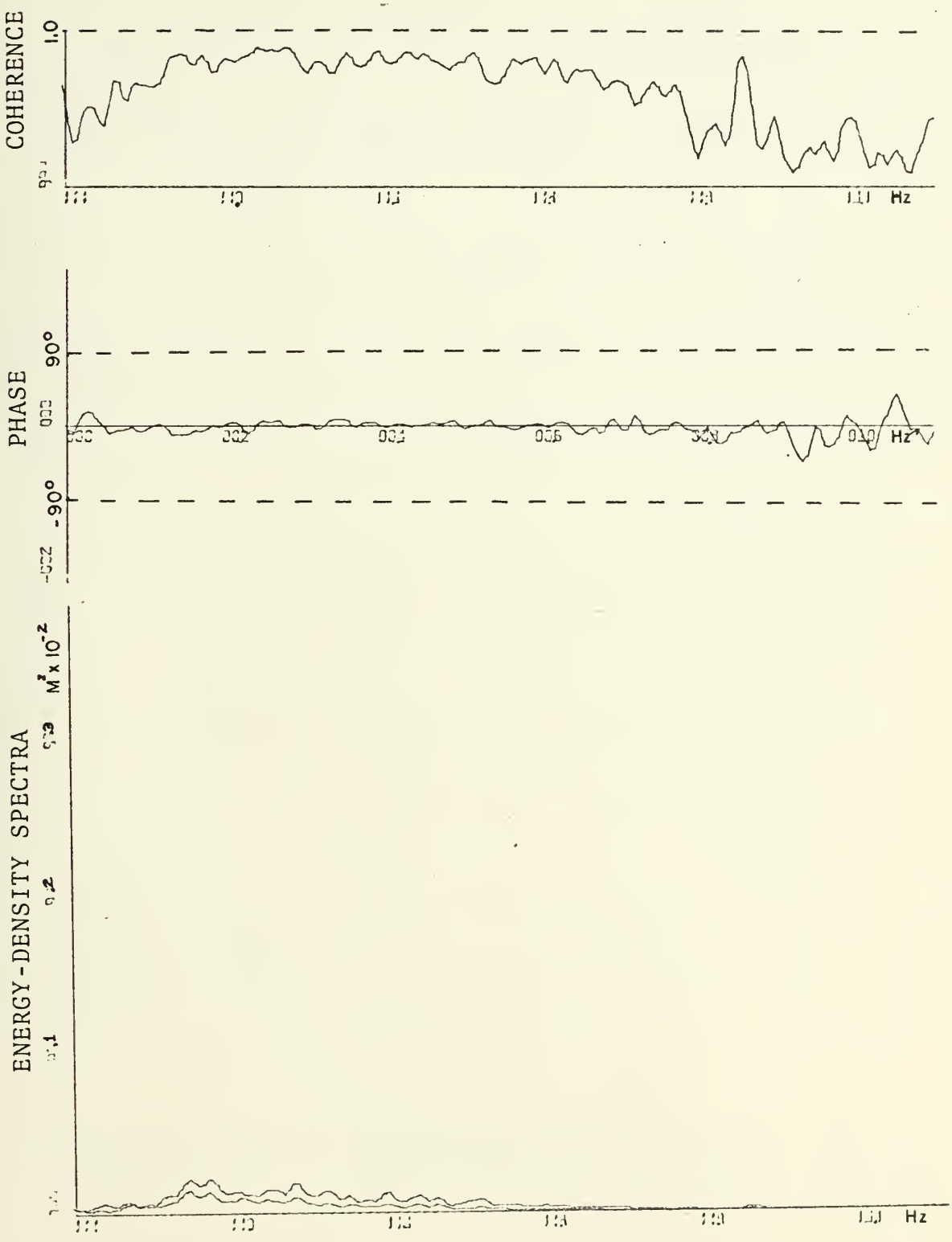

Spectra of Vertical Particle Velocity at Depth 39 cm and Vertical Particle Velocity at Depth 69 cm.

Figure 23

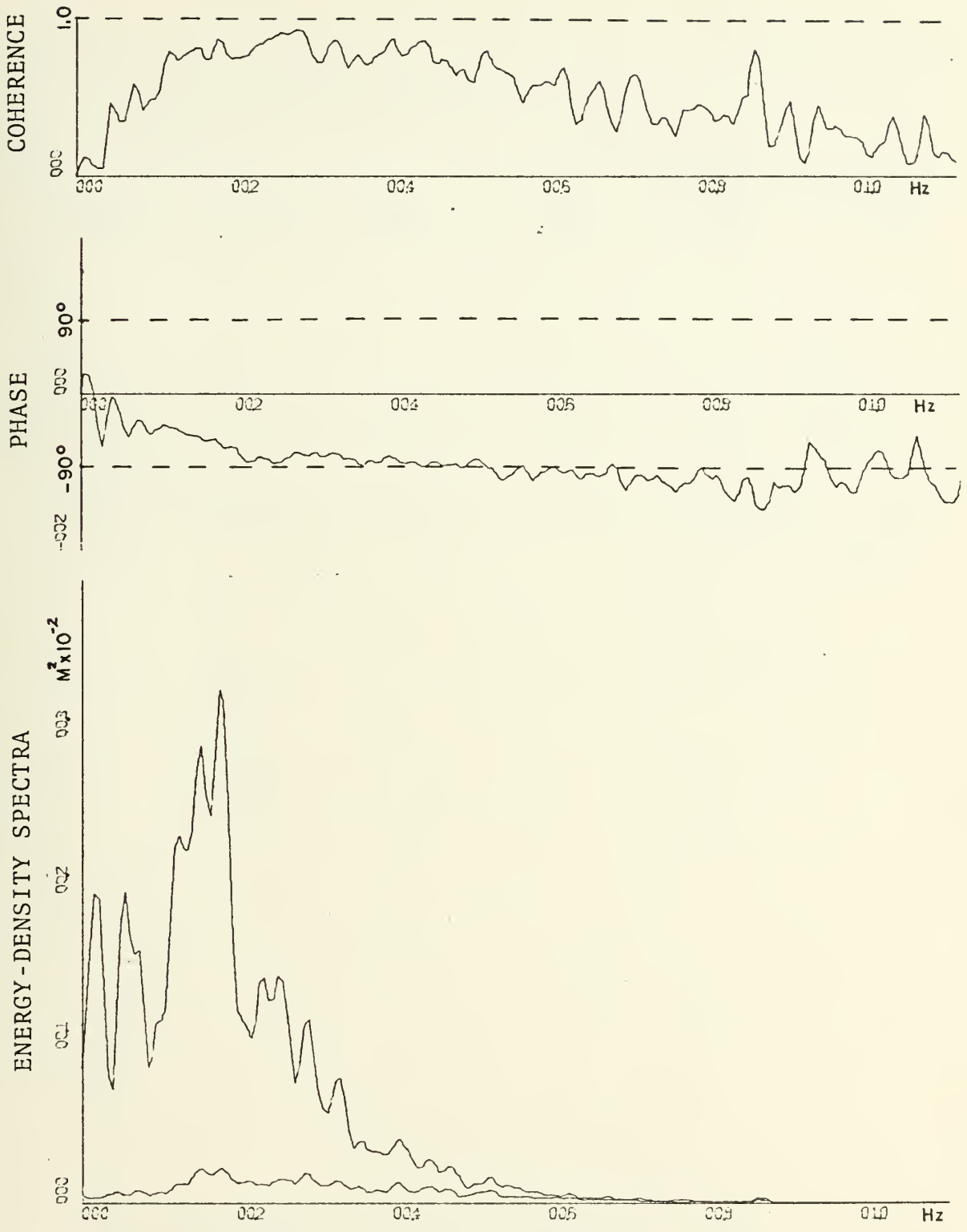

Spectra of Horizontal and Vertical Velocities at Depth 39 cm.

Figure 24

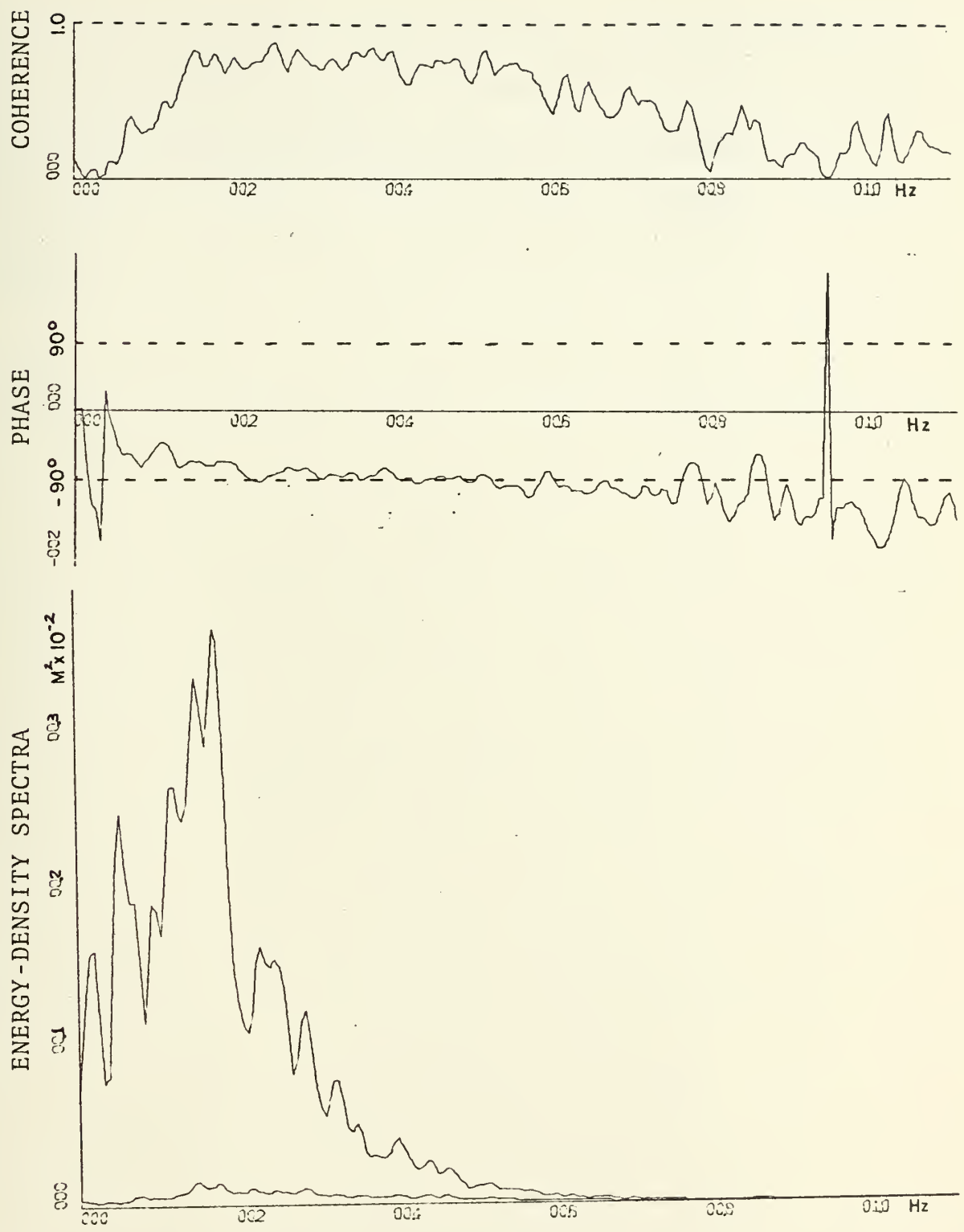

Spectra of Horizontal and Vertical Velocities at Depth 69 cm.

Figure 25

of -90 degrees predicted by linear wave theory, but the phase shift of the horizontal velocity is present at both depths. The difference between the horizontal and vertical kinetic energy at the same depth can be appreciated by the difference between the areas of the energy-density spectra.

VI. CONCLUSIONS

The values of the pdf's show that the asymmetry of the waves after breaking induces asymmetry in both the horizontal and vertical particle velocities.

The good coherence values between the wave record and the different measured velocities indicate that there is a high correlation between these variables; this means that the water particle velocity inside the surf zone is highly wave-induced.

The phase angle was compared to that predicted from linear wave theory. It shows a shifting of phase of the horizontal velocity relative to the sea surface elevation from 0 degree at low frequency to 90 degrees at higher frequencies.

The energy-density spectra show that over 95 percent of the kinetic energy is due to the horizontal water particle velocity. This is in accord with theory for shallow water. The significant total energy is concentrated within a defined range of frequencies corresponding to the wave band; it is inferred that there is a transfer of energy to the turbulent region of the spectra inside the surf zone.

From this the conclusion can be drawn that the flow motion inside the surf zone is not as completely disorganized as it might look, but rather, even after the breaking of the waves the water particle velocities depend on the sea surface shape and follow some determined patterns. More studies are necessary to get a good knowledge of the details particularly for different types of breaking waves.

BIBLIOGRAPHY

1. Bendat, J. S. and A. G. Piersol, Measurement and Analysis of Random Data, John Wiley and Sons, Inc. New York, 1966.

2. Collins, J. I., Probabilities of Wave Characteristics in the Surf Zone, Proceedings of the 12th Coastal Engineering Conference, ASCE, 1970.

3. Inman, D. L. and N. Nasu, Orbital Velocity Associated with Wave Action Near the Breaker Zone, U. S. Army Corps of Engineers, Beach Erosion Board, Technical Memorandum No. 79, March 1956.

4. Iversen, H. W., Waves and Breakers in Shoaling Water, Proc. Third Conf. Coastal Eng., Council on Wave Research, 1-12, 1953.

5. Miller, R. L. and J. M. Zeigler, The Internal Velocity Field in Breaking Waves, 9th Conference on Coastal Engineering, Proceedings ASCE, 1964.

6. Thornton, E. B., A Field Investigation of Sand Transport in the Surf Zone, Proceedings of the 11th Coastal Engineering Conference, ASCE, 1969.

7. Walker, J. R., Estimation of Ocean Wave-Induced Particle Velocities from the Time History of a Bottom Mounted Pressure Transducer, M. S. Thesis, University of Hawaii, 1969.

INITIAL DISTRIBUTION LIST

		No. Copies
1.	Defense Documentation Center Cameron Station Alexandria, Virginia 22314	2
2.	Library, Code 0212 Naval Postgraduate School Monterey, California 93940	2
3.	Department of Oceanography Naval Postgraduate School Monterey, California 93940	3
4.	CDR Leopoldo Salas R. Direccion de Hidrografia y Navegacion Apartado 6745 Caracas, Venezuela	1
5.	Dr. Edward B. Thornton Department of Oceanography Naval Postgraduate School Monterey, California 93940	5
6.	Dr. R. G. Dean Coastal and Oceanographic Engineering Department University of Florida Gainesville, Florida 32601	1
7.	Office of the Oceanographer of the Navy 732 N. Washington Street Alexandria, Virginia 22314	1
8.	Office of Naval Research Code 480 Arlington, Virginia 22217	1
9.	Dr. Vincent Cushing Engineering-Physics Company 12721 Twinbrook Parkway Rockville, Maryland 20852	1

10. Dr. Jacob Van De Kreeke — 1
School of Marine and Atmospheric Sciences
Division of Ocean Engineering
10 Rickenbacker Causeway
Miami, Florida 33149

11. Dr. Douglas L. Inman — 1
Scripps Institute of Oceanography
University of California, San Diego
PO Box 109
La Jolla, California 92038

12. Prof. Joe Johnson — 1
Department of Civil Engineering
412 Hesse Hall
University of California, Berkeley
Berkeley, California 94700

13. Dr. M. S. Longuet-Higgins — 1
National Institute of Oceanography
Wormley, Godalming, Surrey
United Kingdom

14. Director — 1
National Oceanic and Atmospheric Administration
U. S. Department of Commerce
Washington, D.C. 20235

15. Chief of Naval Research — 1
Geography Branch, Code 414
Office of Naval Research
Washington, D.C. 20360

16. Director — 1
Coastal Engineering Research Center
Corps of Engineers, U. S. Army
5201 Little Falls Road, N.W.
Washington, D.C. 20315

17. Mr. Rudolf Savage — 1
Coastal Engineering Research Center
Corps of Engineers, U. S. Army
5201 Little Falls Road, N.W.
Washington, D.C. 20315

18. Dr. D. L. Harris — 1
Coastal Engineering Research Center
Corps of Engineers, U. S. Army
5201 Little Falls Road, N.W.
Washington, D. C. 20315

19. Dr. Julian Gomez — 1
Instituto Espanol De Oceanografia
Alcala 27
Madrid 14, Spain

20. Dr. Cesar Vargas Faucheaux — 1
B. Salcedo No. 541-201
Lince, Lima, Peru

21. Dr. Alejandro Villalobos — 1
Instituto De Biologia
AP. Postal 70-233
Mexico 20 D.F., Mexico

22. Sr. Doctor — 1
Decano Facultad Ciencias Del Mar
Universidad Jorge Tadeo Lozano
Bogota, Colombia

23. Sr. Almirante — 1
Comandante Armada Nacional
Comando Armada Edificio C.A.N.
Bogota, Colombia

24. Sr. Contralmirante — 1
Director Marina Mercante
Comando Armada - Edificio C.A.N.
Bogota, Colombia

25. Sr. Capitan De Fragata — 1
Jefe de Estudios Escuela Naval
Escuela Naval de Colombia
Cartagena, Colombia

26. Dr. Warren C. Thompson — 1
Oceanography Department
Naval Postgraduate School
Monterey, California 93940

27. Teniente De Fragata — 5
Rafael Steer
Calle 70 No. 59-15
Barranquilla, Colombia

Security Classification

DOCUMENT CONTROL DATA - R & D

(Security classification of title, body of abstract and indexing annotation must be entered when the overall report is classified)

ORIGINATING ACTIVITY (Corporate author)	2a. REPORT SECURITY CLASSIFICATION
Naval Postgraduate School Monterey, California 93940	2b. GROUP

REPORT TITLE

Kinematics of Water Particle Motion Within the Surf Zone

DESCRIPTIVE NOTES (Type of report and inclusive dates)

Master's Thesis; September 1972

AUTHOR(S) (First name, middle initial, last name)

Rafael Steer

REPORT DATE	7a. TOTAL NO. OF PAGES	7b. NO. OF REFS
September 1972	61	7

a. CONTRACT OR GRANT NO.	9a. ORIGINATOR'S REPORT NUMBER(S)
b. PROJECT NO.	
c.	9b. OTHER REPORT NO(S) (Any other numbers that may be assigned this report)
d	

10 DISTRIBUTION STATEMENT

Approved for public release; distribution unlimited

11 SUPPLEMENTARY NOTES	12. SPONSORING MILITARY ACTIVITY
	Naval Postgraduate School Monterey, California 93940

13 ABSTRACT

Simultaneous measurements of sea surface elevation and horizontal and vertical particle velocities at 39 and 69 cm elevations in the comumn of water of 130 cm total depth were made inside the surf zone. Also, the offshore sea surface elevation at this location was measured for purposes of comparison. The velocities were measured using electro-magnetic flow meters, and the sea surface elevation was measured using pressure wave gauges. Probability density functions, pdf, were determined for each record. The pdf's for the sea surface elevation and particle velocities inside the surf zone were highly skewed. Spectral computations show that the range of significant energy was between 0.05 and 0.6 hertz. The phase angle was compared to linear wave theory and shows a shifting of phase for the horizontal velocity with sea surface elevation from 0 degree at low frequency to 90 degrees at higher frequencies. The energy-density spectra show that the horizontal component is approximately 95% of the total kinetic energy of the surf zone. In the range of significant energy, a coherence of about 0.9 was found for the sea surface elevation and particle velocities which indicates that the particle motion inside the surf zone is for the most part wave-induced.

DD FORM 1 NOV 65 1473 (PAGE 1)

S/N 0101-807-6811

Security Classification

A-31408

14. KEY WORDS	LINK A		LINK B		LINK C	
	ROLE	WT	ROLE	WT	ROLE	WT
Breaking Waves						
Surf Zone						
Water Particle Velocities						
Electromagnetic Flow Meter						

n